

# Tyche: Stochastic In-Context Learning for Medical Image Segmentation

Marianne Rakic  
CSAIL MIT  
Broad Institute  
m.rakic@mit.edu

Hallee E. Wong  
CSAIL MIT & MGH

Jose Javier Gonzalez Ortiz  
MosaicML DataBricks  
& MIT

Beth Cimini  
Broad Institute

John Guttag  
CSAIL MIT

Adrian V. Dalca  
CSAIL MIT  
& HMS, MGH

## Abstract

*Existing learning-based solutions to medical image segmentation have two important shortcomings. First, for most new segmentation task, a new model has to be trained or fine-tuned. This requires extensive resources and machine-learning expertise, and is therefore often infeasible for medical researchers and clinicians. Second, most existing segmentation methods produce a single deterministic segmentation mask for a given image. In practice however, there is often considerable uncertainty about what constitutes the correct segmentation, and different expert annotators will often segment the same image differently. We tackle both of these problems with Tyche, a model that uses a context set to generate stochastic predictions for previously unseen tasks without the need to retrain. Tyche differs from other in-context segmentation methods in two important ways. (1) We introduce a novel convolution block architecture that enables interactions among predictions. (2) We introduce in-context test-time augmentation, a new mechanism to provide prediction stochasticity. When combined with appropriate model design and loss functions, Tyche can predict a set of plausible diverse segmentation candidates for new or unseen medical images and segmentation tasks without the need to retrain. Code available at: <https://github.com/mariannerakic/tyche/>.*

## 1. Introduction

Segmentation is a core step in medical image analysis, for both research and clinical applications. However, current approaches to medical image segmentation fall short in two key areas. First, segmentation typically involves training a

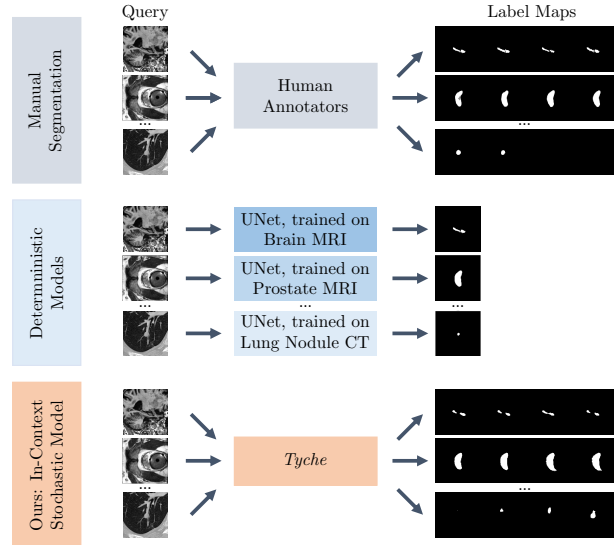


Figure 1. **Tyche: the first in-context stochastic segmentation framework.** Human annotators (top) can handle a wide variety of tasks, and different annotators often produce differing segmentations. Existing automated methods (middle) are typically task-specific and provide only one segmentation per image. *Tyche* (bottom) can capture the disagreement among annotators across many modalities and anatomies without retraining or fine-tuning.

new model for each new modality and biomedical domain, which quickly becomes infeasible given the resources and expertise available in biomedical research and clinical environments. Second, models most often provide a single solution, whereas in many cases, the target image contains ambiguous regions, and there isn't a *single* correct segmentation. This ambiguity can arise from noisy or low contrast images, variation in the task definition, or human raters' in-

terpretations and downstream goals [12, 55]. Failure to take this ambiguity into account can affect downstream analysis, diagnosis, and treatment.

Recent work tackles these issues separately. *In-context learning* methods generalize to unseen medical image segmentation tasks, employing an input *context* or *prompt* to guide inference [19, 128, 129]. These methods are deterministic and predict a *single* segmentation for a given input image and task.

Separately, stochastic or probabilistic segmentation methods output multiple plausible segmentations at inference, reflecting the task uncertainty [11, 67, 95]. Each such model is trained for a specific task, and can only output multiple plausible segmentations at inference for that task. Training or fine-tuning a model for a new task requires technical expertise and computational resources that are often unavailable in biomedical settings.

We present *Tyche*, a framework for stochastic in-context medical image segmentation (Figure 1). *Tyche* includes two variants for different settings. The first, *Tyche-TS* (Train-time Stochasticity), is a system explicitly designed to produce multiple candidate segmentations. The second, *Tyche-IS* (Inference-time Stochasticity), is a test time solution that leverages a pretrained deterministic in-context model.

*Tyche* takes as input the image to be segmented (target), and a *context set* of image-segmentation pairs that defines the task. This enables the model to perform unseen segmentation tasks upon deployment, omitting the need to train new models. *Tyche-TS* learns a *distribution of possible label maps*, and predicts a set of plausible stochastic segmentations. *Tyche-TS* encourages *diverse* predictions by enabling the internal representations of the different predictions to interact with each other through a novel convolutional mechanism, a carefully chosen loss function and noise as an additional input. In *Tyche-IS*, we show that applying test time augmentation to both the target and context set in combination with a trained in-context model leads to competitive segmentation candidates.

We make the following contributions.

- We present the first solution for probabilistic segmentation for in-context learning. We develop two variants to our framework: *Tyche-TS* that is trained to maximize the quality of the best prediction, and *Tyche-IS*, that can be used straightaway with an existing in-context model.
- For *Tyche-TS*, we introduce a new mechanism, *SetBlock*, to encourage diverse segmentation candidates. Simpler than existing stochastic methods, *Tyche-TS* predicts all the segmentation candidates in a single forward pass.
- Through rigorous experiments and ablations on a set of twenty unseen medical imaging tasks, we show that both frameworks produce solutions that outperform existing in-context and interactive segmentation benchmarks, and can match the performance of specialized stochastic net-

works trained on specific datasets.

## 2. Related Work

Biomedical segmentation is a widely-studied problem, with recent methods dominated by UNet-like architectures [6, 51, 107]. These models tackle a wide variety of tasks, such as different anatomical regions, different structures to segment within a region, different image modalities, and different image settings. With most methods, a new model has to be trained or fine-tuned for each combination of these. Additionally, most models don't take into account image ambiguity, and provide a single deterministic output.

**Multiple Predictions.** Uncertainty estimation can help users decide how much faith to put in a segmentation [26] and guide downstream tasks. Uncertainty is often categorized into aleatoric, uncertainty in the data, and epistemic, uncertainty in the model [29, 61]. In this work, we focus on aleatoric uncertainty. Medical images are also heteroscedastic in that the degree of uncertainty varies across the image.

Different strategies exist to capture uncertainty. One can assign a probability to each pixel [45, 52, 62, 76], or use contour strategies and difference loss functions to predict the largest and smallest plausible segmentations [73, 132]. These strategies however do not capture the correlations across pixels. To address this, some methods generate multiple plausible label maps given an image [11, 67, 68, 95, 130]. To achieve this, one can directly model pixel correlations, such as through a multivariate Gaussian distribution (with low rank) covariance [95], or more complex distributions [15]. Alternatively, various frameworks combine potentially hierarchical representations for UNet-like architectures with variational auto-encoders [11, 67, 68]. More recently, diffusion models have been used for ensembling [130] or to produce stochastic segmentations [105, 133]. Some methods explicitly model the different annotators to capture ambiguity [48, 100, 111, 124]. But these methods do not apply to our framework where the number of annotators and their characteristics are unknown.

Most of the models above involve sophisticated modeling or lengthy runtimes, and need to be trained on each segmentation task. In *Tyche*, we build on intuition across these methods, but combine a more efficient mechanism with an in-context strategy to predict segmentation candidates.

**In-context Learning.** Few-Shot frameworks use a small set of examples to generalize to new tasks [31, 80, 98, 101, 113, 117, 134], sometimes by fine-tuning an existing pretrained model [32, 99, 120, 125]. In-context learning segmentation methods (ICL) use a small set of examples directly as input to infer label maps for a task [9, 19, 63, 63, 129, 129]. This enables them to generalize to new tasks. For example, UniVerSeg uses an enhanced UNet-based architecture to gen-

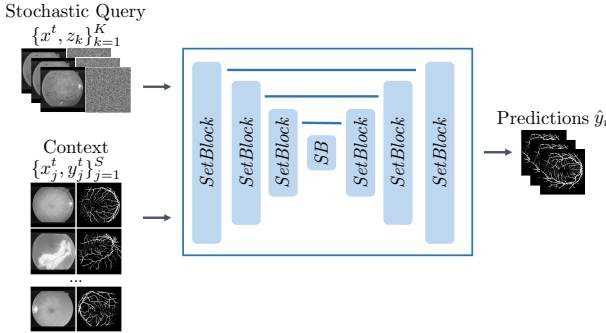


Figure 2. **Tyche Model Schematic.** The target  $x^t$ , context set  $(x_j^t, y_j^t)_{j=1}^S$ , and noise images  $\{z_k\}_{k=1}^K$  are inputs to the network. The architecture employs UNet-like levels, but uses *SetBlocks* that enable interactions between the context set and the target segmentation candidates.

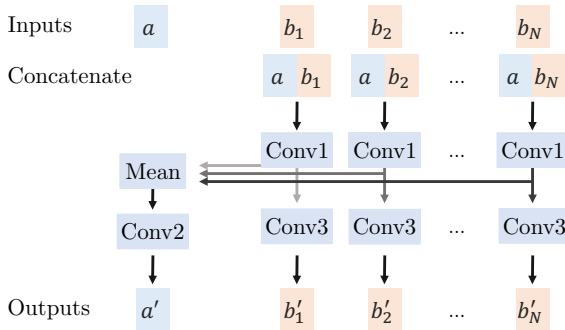


Figure 3. **CrossBlock Mechanism** The CrossBlock involves interactions between a single feature and a set of features and outputs new feature for the target and new features for each.

eralize to medical image segmentation tasks unseen during training [19]. We build on these ideas to enable segmentation of new tasks without the need to re-train, but expand this paradigm to model stochastic segmentations.

**Test Time Augmentation.** The test-time augmentation (TTA) strategy uses perturbations of a test input and ensembles the resulting predictions. Existing TTA frameworks model accuracy [33, 64, 116, 119], robustness [25], and estimates of uncertainty [5, 90]. Test-time augmentation has been applied to diverse anatomies and modalities including brain MRI and retinal fundus [3, 5, 49, 53, 97, 127]. Prior work has formalized the variance of a model’s predictions over a set of input transformations as capturing aleatoric uncertainty [5, 126, 127].

*Tyche*’s use of TTA is distinct from prior work. Instead of ensembling segmentations over perturbations of a test input or pixel-wise estimates of uncertainty, *Tyche* extends TTA to the in-context setting and uses the individual TTA predictions to model uncertainty.

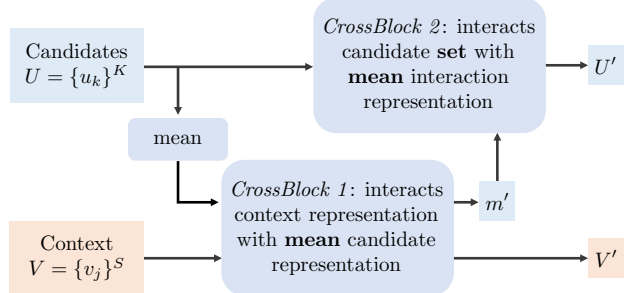


Figure 4. **SetBlock Mechanism.** *SetBlock* enables interactions between the set of features from the context set and the set of features from the prediction candidates. It outputs two sets of features, one for the context and one for the prediction candidates.

### 3. Method

For segmentation task  $t$ , let  $\{(x_j^t, y_j^t)\}_{j=1}^N$  be a dataset with images  $x^t$  and label maps  $y^t$ . Typical segmentation models learn a different function  $\hat{y}^t = g_{\theta^t}(x^t)$  with parameters  $\theta^t$  for each task  $t$ , where  $\hat{y}^t$  is a single segmentation map prediction.

We design *Tyche* as an in-context learning (ICL) model using a *single* function for all tasks:

$$\hat{y}_k^t = f_{\theta}(x^t, z_k, \mathcal{S}^t). \quad (1)$$

This function, with *global* parameters  $\theta$ , captures a *distribution of label maps*  $\{\hat{y}_k^t\}_{k=1}^K$ , given target  $x^t$ , context set  $\mathcal{S}^t = \{x_j^t, y_j^t\}_{j=1}^S$  defining task  $t$ , and noise  $z_k \sim \mathcal{N}(\mathbf{0}, \mathbb{I})$ . We use this modelling strategy in two ways: we either explicitly train a network to approximate the model  $f_{\theta}(\cdot)$  in *Tyche-TS*, or design a test-time strategy to approximate  $f_{\theta}(\cdot)$  using an existing (pretrained) deterministic in-context network in *Tyche-IS*.

#### 3.1. Tyche-TS

In *Tyche-TS*, we explicitly train a neural network for  $f_{\theta}(\cdot)$  that can make different predictions given the same image input  $x^t$  but different noise channels  $z_k$ . We model interaction between predictions, and employ a loss that encourages diverse solutions (Figure 2).

##### 3.1.1 Neural Network

We use a convolutional architecture focused on interacting representations of sets of flexible sizes using a modified version of the usual UNet structure [107].

**Inputs.** *Tyche-TS* takes as input the target  $x^t$ , a set of  $K$  Gaussian noise channels  $z_k$ , and a context set,  $\mathcal{S}^t$ .

**Layers.** Each level of the UNet takes as input a set of  $K$  candidate representations and  $S$  context representations. We design each level to encourage communication between the

intermediate elements of the sets, and between the two features of the segmentation candidates. The size  $K$  is flexible and can vary with iterations.

**SetBlock.** We introduce a new operation called *SetBlock*, which interacts the candidate representations  $U = \{u_i\}_{i=1}^K$ , with the context representations  $V = \{v_i\}_{i=1}^S$ , illustrated in Figure 4. We use the *CrossBlock* [19] as a building block for this new layer. The  $\text{CrossBlock}(u, V) \rightarrow (u', V')$  compares an image representation  $u$  to a context set representation  $V$  through convolutional and averaging operations, and outputs a new image representation  $u'$  and a new set representation  $V'$  (Figure 3).  $\text{SetBlock}(U, V) \rightarrow (U', V')$  builds on *CrossBlock* and performs a set to set interaction of the entries of  $U$  and  $V$ :

$$\bar{u} = 1/m \sum_{i=1}^m u_i \quad (2)$$

$$\bar{u}', V' = \text{CrossBlock}(\bar{u}, V) \quad (3)$$

$$u'_i = \text{Conv}_m(u_i || \bar{u}'), \quad i = 1, \dots, K \quad (4)$$

$$u'_i = \text{Conv}_u(u'_i), \quad i = 1, \dots, K \quad (5)$$

$$v'_i = \text{Conv}_v(v_i), \quad i = 1, \dots, S, \quad (6)$$

where  $||$  is the concatenation operation along the feature dimension. The *CrossBlock* interacts the context representation with the **mean** candidate. The  $\text{Conv}_m$  step communicates this result to all candidate representation.  $\text{Conv}_u$  and  $\text{Conv}_v$  then update all representations. All convolution operations include a non-linear activation function.

### 3.1.2 Best candidate Loss

Typical loss function compute the loss of a single prediction relative to a single target, but *Tyche-TS* produces multiple predictions and has one or more corresponding label maps. We optimize

$$\mathcal{L}(\theta; \mathcal{T}) = \mathbb{E}_{t \in \mathcal{T}} [\mathbb{E}_{(x^t, y_r^t), \mathcal{S}^t} [\mathcal{L}_{seg}(\{\hat{y}_k\}, y_r^t)]], \quad (7)$$

with

$$\mathcal{L}_{seg}(\{\hat{y}_k\}, y) = \min_k \mathcal{L}_{Dice}(y_k, y), \quad (8)$$

where  $y_r^t$  is a segmentation from rater  $r$ , and  $\mathcal{L}_{Dice}$  is a weighted sum of soft Dice loss [94] and categorical cross-entropy. By only back-propagating through the best prediction among  $K$  candidates, the network is encouraged to produce diverse solutions [22, 41, 66, 81].

### 3.1.3 Training Data

We employ a large dataset of single- and multi-rater segmentations across diverse biomedical domains. We then use data augmentation [19], as described in B.3.

We add synthetic multi-annotator data by modelling an image as the average of four blobs representing four raters (Figure 10). Each blob is white disk  $b_i$  deformed by a random smoothed deformation field  $\phi_i$ . The synthetic image is

a noisy weighted sum of raters:  $\sum_{i=1}^4 w_i(b_i \circ \phi_i)$  where  $\circ$  represents the spacial warp operation.

### 3.1.4 Implementation Details

We use a UNet-like architecture of 4 *SetBlock* layers for the encoder and decoder, with 64 features each and Leaky ReLU as activation function. We use the Adam optimizer and a learning rate of 0.0001. At training, we have a fixed number of candidates per sample  $K_{tr} = 8$ . At inference, we consider different numbers of candidates.

## 3.2. Tyche-IS

In *Tyche-IS*, we first train (or use an existing trained) *deterministic* in-context segmentation system:

$$\hat{y}^t = h_\theta(x^t, \mathcal{S}^t).$$

We then introduce a *test-time* in-context augmentation strategy to provide stochastic predictions:

$$\hat{y}_k^t = f_\theta(x^t, z_k, \mathcal{S}^t) \quad (9)$$

$$= h_\theta(\text{aug}(x^t, z_k, \mathcal{S}^t)), \quad (10)$$

where  $\tilde{x}^t, \tilde{\mathcal{S}}^t = \text{aug}(x^t, z_k, \mathcal{S}^t)$  is an augmentation function.

### 3.2.1 Augmentation Strategy

Test time augmentation for single task networks  $y = g_t(x)$  applies different transforms to an input image  $x$ :

$$\tilde{x}_k = a_\phi(x, z_k), \quad (11)$$

where  $\phi$  are augmentation parameters and  $z_k$  is a random vector. A final prediction is then obtained by combining several predictions of augmented images. Most commonly, the combining function averages the predictions:

$$y = \frac{1}{k} \sum_k g_t(\tilde{x}_k), \quad (12)$$

where the sum operates pixel-wise.

We introduce in-context test-time augmentation (ICTTA) prediction as another mechanism to generate diverse stochastic predictions.

We apply augmentation to both the test target  $x^t$  and the context set  $\mathcal{S}^t$ :

$$(\tilde{x}_i^t, y_i^t) = (a_\phi(x_i^t), y_i^t) \quad (13)$$

$$\tilde{\mathcal{S}}^t = \{a_\phi(x_j^t), y_j^t\}_{j=1}^S. \quad (14)$$

We repeat this process  $K_i$  times to obtain  $K_i$  stochastic predictions:

$$\hat{y}_k = f_\theta(\tilde{x}_i^t, z_k, \tilde{\mathcal{S}}^t) \quad (15)$$

We only apply intensity based transforms, to avoid the need to invert the segmentations back. We apply Gaussian noise, blurring and pixel intensity inversion. We detail the specific augmentations in B.2.

## 4. Experimental Setup

### 4.1. Data

We evaluate our method using a large collection of biomedical and synthetic datasets. Most datasets include a single manual segmentation for each example, while a few have several raters per image.

**Data Splits.** We partition each dataset into development, validation, and test splits. We assign each dataset to an *in-distribution* set (*I.D.*) or an *out-of-distribution* set (*O.D.*). We train exclusively on the development splits of the *I.D.* datasets, and use the validation splits of the *I.D.* datasets to tune parameters. We use the validation splits of the *O.D.* datasets for final model selection. We report results on the test splits of the *O.D.* datasets.

For each use case, we sample the context from each dataset’s corresponding development set. As a result, the network doesn’t see any of the *O.D.* datasets at training time.

We distinguish between single annotator data and multi-annotator data.

**Single-Annotator Data.** For single annotator data, we build on MegaMedical used in recent publications [19, 131] and employ a collection of 73 datasets, of different public biomedical domains and different modalities [1, 2, 7, 14, 16, 17, 19, 21, 24, 34–36, 39, 40, 42, 43, 50, 54, 56, 57, 59, 69, 71, 72, 74, 75, 77–79, 82–89, 91, 96, 103, 104, 106, 110, 112, 115, 118, 121, 122, 135, 137–139]. MegaMedical spans a variety of anatomies and modalities, including brain MRI, cardiac ultrasound, thoracic CT and dental X-ray. We also use synthetic data involving simulated shapes, intensities, and image artifacts [19, 44]. The single-annotator datasets used for out-of-domain (*O.D.*) testing are: PanDental [1], WBC [139], SCD [104], ACDC [14], and SpineWeb [138].

**Multi-Annotator Data.** For multi-annotator *I.D.* data, we use four datasets from Qubiq [92]: Brain Growth, Brain Lesions, Pancreas Lesions, and Kidney. We also simulate a multi-rater dataset consisting of random shapes (blobs). For the *O.D.* multi-annotator data we use four datasets. One contains hippocampus segmentation maps on brain MRIs from a large hospital. We crop the volumes around the hippocampus [67] to focus on the areas where the raters disagree. The second is a publicly available lung nodule dataset, LIDC-IDRI [4]. This dataset is notable for the substantial inter-rater variability. It contains 1018 thoracic CT scans, each annotated by 4 annotators from a pool of

	In-Context	Stochastic	Automatic
SENet	✓		✓
UniverSeg	✓		✓
SegGPT	✓		✓
Prob. UNet		✓	✓
PhiSeg		✓	✓
CIMD		✓	✓
SAM-based	✓	✓	
<b>Tyche</b>	✓	✓	✓

Table 1. **Summary of evaluated methods used and their properties.** Only *Tyche* is both stochastic and in-context, and does not require user interaction.

12 annotators. Finally, we also use retinal fundus images, STARE [47], annotated by 2 raters, and prostate data from the MICCAI 2021 QUBIQ challenge [92], annotated by 6 raters on two tasks. Single and multi-annotator combined, our *O.D.* group contains 20 tasks unseen at training time (some datasets have several tasks).

### 4.2. Evaluation

We evaluate our method by analysing individual prediction quality and distribution of predictions, both qualitatively and quantitatively. We also examine model choices through an ablation study.

A main use case of stochastic segmentation is to propose a small set of segmentations to a human rater, who can select the most appropriate one for their purpose. For this scenario, a model can be viewed as good if at least one prediction matches what the rater is looking for. We thus employ the best candidate Dice metric.

In the multi-annotator setting, we evaluate using both best candidate Dice score, also called maximum Dice score, as well as Generalized Energy Distance (GED)[13, 109, 123]. GED is commonly used in the stochastic segmentation literature to asses the difference between the distribution of predictions and the distribution of annotations [11, 67, 95, 105, 133]. GED has limitations, such as rewarding excessive prediction diversity [105]. Let  $\mathcal{Y}$  and  $\hat{\mathcal{Y}}$  be the set of annotations, GED is defined as:

$$D_{GED}^2(\mathcal{Y}, \hat{\mathcal{Y}}) = 2\mathbb{E}[d(p, \hat{p})] - \mathbb{E}[d(p, p')] - \mathbb{E}[d(\hat{p}, \hat{p}')], \quad (16)$$

where  $p, p' \sim \mathcal{Y}$ ,  $\hat{p}, \hat{p}' \sim \hat{\mathcal{Y}}$  and  $d(\cdot, \cdot)$  is a distance metric. We use the Dice score [30].

### 4.3. Benchmarks

*Tyche* is the first method to produce stochastic segmentation predictions in-context. Consequently, we compare *Tyche* to existing benchmarks, each of which achieves only a subset of our goals.

**In-Context Methods.** We compare to deterministic frameworks that can leverage a context set: a few-shot method,

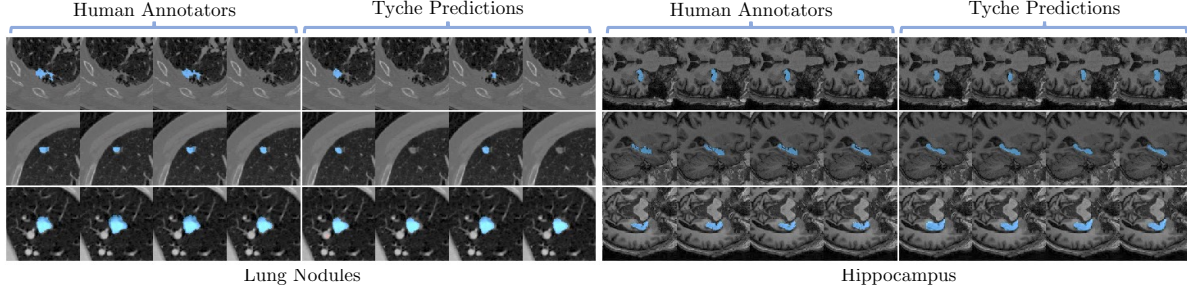


Figure 5. **Visualization of predictions for three different samples**, 1 per row. Left: LIDC-IDRI. Right: Hippocampus dataset. The leftmost columns are raters’ annotations. The 4 last columns are model predictions. *Tyche* provides a set of prediction that is diverse and matches the raters, for tasks unseen at training time.

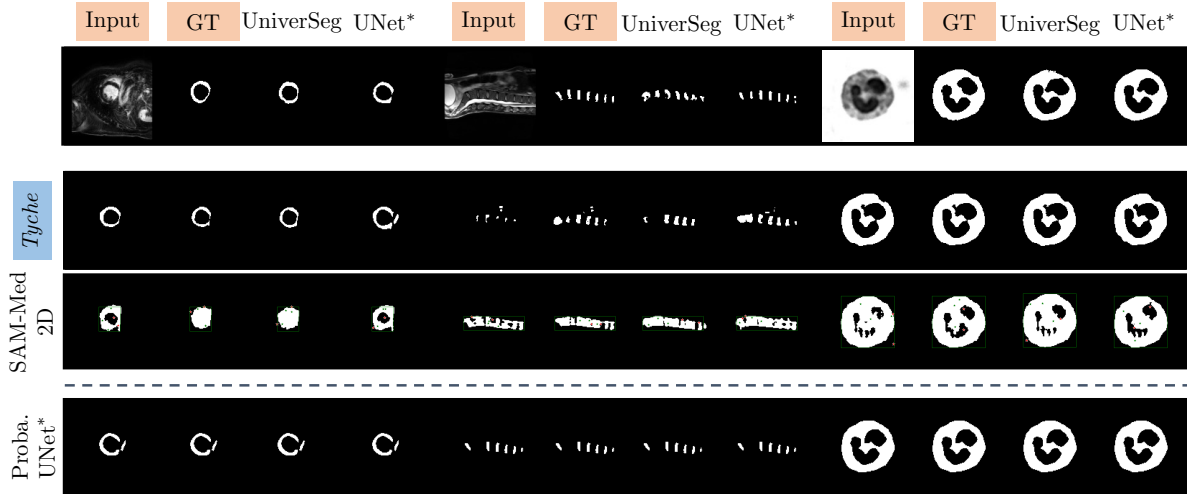


Figure 6. **Single annotator visualization for different models.** We show three example images that show very different corresponding segmentation. *Tyche* can output plausible segmentation for single annotator data with varying degrees of variability in the segmentation. Methods with an asterisk are upper baselines.

SENet [108], and two in-context learning (ICL) methods, UniverSeg [19] and SegGPT [129]. We train UniverSeg and SENet with the same data split strategies and the same sets of augmentation transforms as for *Tyche*. For SegGPT, we use the public model, trained on a mix of natural and medical images. Figure 13 in the Supplemental Material shows that UniverSeg trained with additional data outperforms its public version.

**Stochastic Upper Bounds.** We compare to task-specialized probabilistic segmentation methods that are trained-on and perform well on specific datasets. We independently train Probabilistic UNet [67], PhiSeg[11] and CIDM, a recent diffusion network [105], on each of the 20 held-out tasks. For each task, we train three model variants: no augmentation, weak augmentation, and as much augmentation as for the *Tyche* targets. For each benchmark variant, we train on a *O.D.* development split and select the model that performs best on the corresponding *O.D.* validation split. We then

compare these benchmarks to *Tyche* on the held-out *O.D.* test splits.

These models are explicitly optimized for the datasets on which they are evaluated, unlike *Tyche*, which does not use those datasets for training. Since these are trained, tuned and evaluated on the *O.D.* datasets splits, something we explicitly aim to avoid in the problem set up as it is not easily done in many medical settings, they serve as upper bounds on performance.

**Interactive Segmentation Methods.** We compare to two interactive methods: SAM [66] and SAM-Med2D [23]. These methods can provide multiple segmentations, but, unlike *Tyche*, require human interaction, which is outside our scope. SAM also has a functionality to segment all elements in an image, however less optimized for medical imaging. We assume that the SAM-based models have access to the same information as the ICL methods: several image-segmentation pairs as context to guide the segmen-

tation task. We fine-tune SAM using our *I.D.* development datasets. To replace the human interaction, we provide a bounding box, the average context label map, and 10 clicks, 5 positive and 5 negative as input. With SAM-Med2D, we use a bounding box, and several positive and negative clicks as input. For both SAM and SAM-Med2D, we generate clicks and bounding box from the average context label map.

We use one iteration of interaction, and sample different plausible segmentation candidates by sampling different sets of clicks and different averaged context sets.

Table 1 summarizes the features of all the methods. Additional information on the benchmarks is provided in the Supplemental Material.

#### 4.4. Experiments

We evaluate all models on the multi-annotator and single-annotator *O.D.* data. We then analyze the *Tyche* variants individually and perform an ablation study on each to validate parameter choices. Finally, we compare the GPU inference runtimes and model parameters.

In the Supplemental Material, we analyze further the noise given as input, the context set, the number of predictions, the *SetBlock* and the candidate loss. We also provide additional performance metrics and per dataset results. We also compare the performance of *Tyche* and PhiSeg in a few-shot setting. Finally, we provide additional visualizations.

**Inference Setting.** We use a fixed context of 16 image-segmentation pairs, because existing in-context learning systems show minimal improvements beyond this size [19]. Because there is variability in performance depending on the context sampled, we sample 5 different context sets for each datapoint and average performance. Similarly, for the stochastic upper bounds and interactive methods, we do 5 rounds of sampling  $K_i$  samples.

## 5. Results

### 5.1. Comparison to Benchmarks

**Multi-Annotator O.D. Data.** We evaluate on the datasets where *multiple annotations* exist for each sample. Figure 5 shows that, for both the lung nodules and the hippocampus datasets, *Tyche* predictions are diverse and capture rarer diversity, even though these datasets are out-of-domain. Tables 2 and 3 show that both versions of *Tyche* outperform the interactive and deterministic benchmarks on all datasets except for Prostate Task 1, on which SegGPT has similar performance. Using a paired Student t-test, we find that *Tyche-TS* outperforms *Tyche-IS* in terms of maximum Dice score, with  $p < 10^{-10}$ . We find no statistical difference between the two methods in terms of GED.

**Single-Annotator Data.** Figure 6 shows examples of pre-

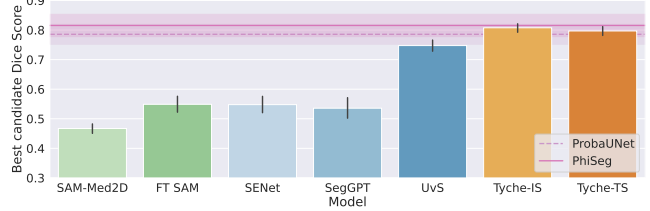


Figure 7. **Best candidate Dice Score for single annotator data aggregated per task.** *Tyche* outperforms the in-context and interactive segmentation benchmarks, and approaches the stochastic upper bounds. Error bars represent the 95% confidence interval.

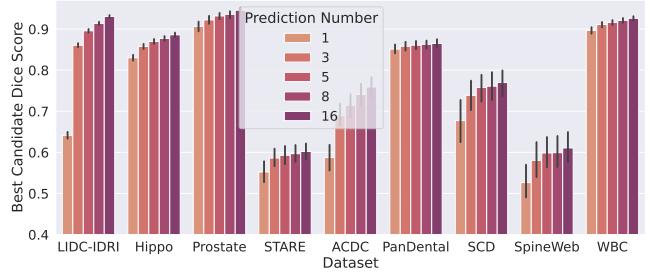


Figure 8. **Best candidate Dice Score as the number of candidate prediction increases.** The largest improvements are usually obtained for a small number of predictions. The error bars represent the 95% confidence interval.

dictions for *Tyche* and the corresponding benchmarks for the single-annotator datasets. *Tyche* produces a more diverse set of candidates than its competitors. Figure 7 compares all plausible models in terms of aggregate best candidate Dice score, except for CIDM, which underperformed for single-annotator data with a mean best candidate Dice score of:  $0.673 \pm 0.032$ . For clarity, we only present the full Figure in the Supplemental Material. *Tyche* performs better than the deterministic and interactive frameworks, and similarly to Probabilistic UNet, one of the upper bound benchmarks that is trained on the O.D. data. A paired Student t-test shows that *Tyche-IS* produces statistically higher GED ( $p = 0.044$ ) than *Tyche-TS*, but we find no statistical difference in terms of best candidate Dice. We hypothesize that *Tyche-IS* is competitive because of the implicit annotator characterization provided by the context.

### 5.2. Tyche Analysis

We analyze *Tyche* variants and study the influence of two important parameters: the number of inference-time candidate predictions  $K_i$  and the size of the context set  $\|\mathcal{S}\|$ .

**Influence of the number of prediction  $K_i$ .** We study how the number of predictions impacts the best candidate Dice score, keeping the context size constant. Figure 8 shows that for *Tyche-TS*, the best candidate Dice score rises with the number of predictions, but with diminishing returns.

$GED^2 (\downarrow)$		Hippocampus	LIDC-IDRI	Prostate Task 1	Prostate Task 2	STARE
Interactive	SAM	0.57 ± 0.02	0.90 ± 0.01	0.20 ± 0.03	0.31 ± 0.06	0.89 ± 0.06
	SAM-Med2d	0.93 ± 0.02	1.01 ± 0.01	0.80 ± 0.09	0.78 ± 0.11	1.52 ± 0.05
I-C & Stochastic (Ours)	Tyche-IS	<b>0.21 ± 0.01</b>	0.41 ± 0.01	0.12 ± 0.02	0.20 ± 0.05	0.73 ± 0.03
	Tyche-TS	0.22 ± 0.01	<b>0.40 ± 0.01</b>	<b>0.09 ± 0.02</b>	<b>0.15 ± 0.03</b>	<b>0.62 ± 0.03</b>
Stochastic Upper Bound	PhiSeg	0.14 ± 0.01	0.33 ± 0.01	0.12 ± 0.01	0.17 ± 0.05	1.22 ± 0.02
	ProbaUNet	0.13 ± 0.01	0.51 ± 0.01	0.08 ± 0.01	0.18 ± 0.05	0.76 ± 0.06
	CIDM	0.17 ± 0.01	0.42 ± 0.01	0.14 ± 0.02	0.26 ± 0.04	0.87 ± 0.05

Table 2. **Generalized Energy Distance** for different models with a context size of 16 for in-context methods and a number of predictions set to 8. Lower is better. *Tyche* outperforms interactive and in-context baselines, and matches stochastic upper bounds.

Max Dice ( $\uparrow$ )		Hippocampus	LIDC-IDRI	Prostate Task 1	Prostate Task 2	STARE
In-Context	UniverSeg	0.84 ± 0.01	0.67 ± 0.01	0.91 ± 0.01	0.88 ± 0.03	0.51 ± 0.02
	SegGPT	0.10 ± 0.01	0.68 ± 0.01	0.94 ± 0.01	0.89 ± 0.03	0.02 ± 0.01
	SENet	0.68 ± 0.01	0.00 ± 0.00	0.83 ± 0.02	0.83 ± 0.02	0.30 ± 0.03
Interactive	SAM	0.71 ± 0.01	0.55 ± 0.01	0.90 ± 0.01	0.85 ± 0.03	0.50 ± 0.03
	SAM-Med2d	0.52 ± 0.01	0.42 ± 0.01	0.62 ± 0.04	0.64 ± 0.06	0.21 ± 0.03
I-C & Stochastic (Ours)	Tyche-IS	0.87 ± 0.01	0.90 ± 0.00	0.94 ± 0.01	0.91 ± 0.01	0.52 ± 0.03
	Tyche-TS	<b>0.88 ± 0.01</b>	<b>0.91 ± 0.00</b>	<b>0.95 ± 0.01</b>	<b>0.93 ± 0.01</b>	<b>0.60 ± 0.02</b>
Stochastic Upper Bound	PhiSeg	0.88 ± 0.00	0.91 ± 0.00	0.93 ± 0.01	0.91 ± 0.02	0.15 ± 0.01
	ProbaUNet	0.91 ± 0.00	0.86 ± 0.01	0.95 ± 0.00	0.91 ± 0.03	0.59 ± 0.02
	CIMD	0.84 ± 0.01	0.92 ± 0.00	0.93 ± 0.01	0.87 ± 0.02	0.41 ± 0.04

Table 3. **Best candidate Dice score** for different models with a context size of 16 for in-context methods and a number of predictions set to 8. Higher is better. *Tyche* outperforms interactive and in-context baselines, and matches stochastic upper bounds.

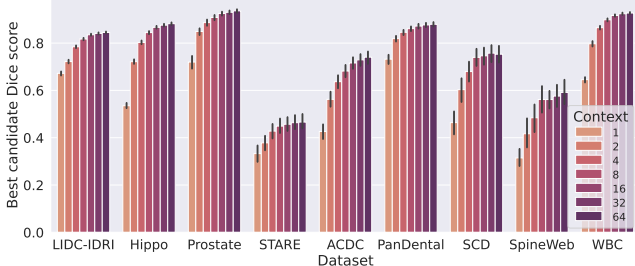


Figure 9. **Best candidate Dice Score per dataset as context size increases.** A context size of 16 is already large enough to obtain a reasonable best candidate Dice. The error bars represent the 95% confidence interval.

**Influence of context size  $\|\mathcal{S}\|$ .** Figure 9 shows that *Tyche-TS* is capable of leveraging the increased context size to improve its best candidate Dice score, and that a context size of 16 is sufficient to achieve most of the gain.

**Ablation.** Table 4 illustrates several ablations on *Tyche* design choices. For *Tyche-TS*, we evaluate the following variants: no simulated multi-annotator images, no *SetBlock* and finally, using the standard deviation of candidate feature representations in addition to the mean in the *SetBlock* (“Std”). We compare the models using best candidate Dice

Blob	SetBlock	Std	Max. DSC( $\uparrow$ )	$GED^2 (\downarrow)$
X			0.810 ± 0.01	0.349 ± 0.04
	X		0.771 ± 0.02	0.425 ± 0.05
		✓	0.802 ± 0.01	0.425 ± 0.05
✓	✓		<b>0.811 ± 0.01</b>	<b>0.298 ± 0.03</b>
Target	CS	CS+	Max. DSC( $\uparrow$ )	$GED^2 (\downarrow)$
✓			0.776 ± 0.02	0.477 ± 0.04
	✓		0.700 ± 0.02	0.410 ± 0.05
		✓	0.561 ± 0.02	0.867 ± 0.05
✓	✓		<b>0.813 ± 0.01</b>	<b>0.333 ± 0.04</b>
✓	✓	✓	0.808 ± 0.01	0.358 ± 0.04

Table 4. **Ablation Study for Tyche variants.** Top: *Tyche-TS*, without simulated multi-annotator data, with *SetBlock*, with Standard Deviation in *SetBlock*. Bottom: *Tyche TeS*, with Target, Context and Large Context augmentations.

averaged across tasks.

Table 4 shows that the simulated multi-annotator data provides negligible improvement, as does adding the standard deviation. However, *SetBlock* is a crucial part to improve the best candidate Dice score.

We study performances for three types of TTA in *Tyche-IS*: on the target, on the context (CS), and on the context while also including the non-augmented context (CS+):

	Inference Time (ms)	Parameters
UniverSeg	$96.62 \pm 0.61$	1.2M
SegGPT	$2857.19 \pm 4.38$	370M
SENet	$14.91 \pm 0.21$	0.89M
FT-SAM	$1036.75 \pm 4.61$	94M
SAM-Med2D	$188.8 \pm 7.58$	91M
PhiSeg	$11.35 \pm 0.672$	21.1M
ProbaUNet	$8.44 \pm 0.46$	5M
CIDM	$1.7 \times 10^5 \pm 2748$	85.6M
<b>Tyche-IS</b>	$128.57 \pm 2.626$	1.2M
<b>Tyche-TS</b>	$18.09 \pm 0.61$	1.7M

Table 5. Inference Runtime and Model Parameters for 8 predictions and a context size of 16.

( $S, \mathcal{G}(S)$ ). Table 4 shows that adding noise to only one of the target and context yields sub-optimal performance, while augmenting both the target and context improves performances.

### 5.3. Inference Runtime

We compare the inference runtime by predicting 8 segmentation candidates with each method, and repeat the process 300 times. We use an NVIDIA V100 GPU. Table 5 shows that *Tyche* is significantly faster and smaller than SegGPT and CIDM, yet, not as fast as some task-specific stochastic models. *Tyche-IS* has fewer parameters than *Tyche-TS*, but needs additional inference time.

## 6. Conclusion

We introduced *Tyche*, the first framework for stochastic in-context segmentation. For any (new) segmentation task, *Tyche* can directly produce diverse segmentation candidates, from which practitioners can select the most suitable one, and draw a better understanding of the underlying uncertainty. *Tyche* can generalize to images from data unseen at training and outperforms in-context and interactive benchmarks. In addition, *Tyche* often matches stochastic models on tasks for which those models have been specifically trained. *Tyche* has two variants, one designed to optimize the best segmentation candidate, with fast inference time, and a test-time augmentation variant that can be used in combination with existing in-context learning methods. We are excited to further study the different types of uncertainty captured by *Tyche-TS* and *Tyche-IS*. We will also extend the capabilities of *Tyche* with more complex support sets, including variable annotators and multiple image modalities.

## 7. Acknowledgement

Research reported in this paper was supported by the National Institute of Biomedical Imaging and Bioengineering of the National Institutes of Health under award number

R01EB033773. This work was also supported in part by funding from the Eric and Wendy Schmidt Center at the Broad Institute of MIT and Harvard as well as Quanta Computer Inc. Finally, some of the computation resources required for this research was performed on computational hardware generously provided by the Massachusetts Life Sciences Center.

## References

- [1] Amir Hossein Abdi, Shohreh Kasaei, and Mojdeh Mehdizadeh. Automatic segmentation of mandible in panoramic x-ray. *Journal of Medical Imaging*, 2(4):044003, 2015. [5](#), [17](#)
- [2] Walid Al-Dhabyan, Mohammed Gomaa, Hussien Khaled, and Aly Fahmy. Dataset of breast ultrasound images. *Data in Brief*, 28:104863, 2020. [5](#), [17](#)
- [3] Mina Amiri, Rupert Brooks, Bahareh Behboodi, and Hassan Rivaz. Two-stage ultrasound image segmentation using u-net and test time augmentation. *International journal of computer assisted radiology and surgery*, 15:981–988, 2020. [3](#)
- [4] Samuel G Armato III and et al. The lung image database consortium (lidc) and image database resource initiative (idri): a completed reference database of lung nodules on ct scans. *Medical physics*, 38(2):915–931, 2011. [5](#), [18](#)
- [5] Murat Seckin Ayhan and Philipp Berens. Test-time data augmentation for estimation of heteroscedastic aleatoric uncertainty in deep neural networks. In *Medical Imaging with Deep Learning*, 2022. [3](#)
- [6] Vijay Badrinarayanan and et al. Segnet: A deep convolutional encoder-decoder architecture for image segmentation. *IEEE transactions on pattern analysis and machine intelligence*, 39(12):2481–2495, 2017. [2](#)
- [7] Ujjwal Baid, Satyam Ghodasara, Suyash Mohan, Michel Bilello, Evan Calabrese, Errol Colak, Keyvan Farahani, Jayashree Kalpathy-Cramer, Felipe C Kitamura, Sarthak Pati, et al. The rsna-asnr-miccai brats 2021 benchmark on brain tumor segmentation and radiogenomic classification. *arXiv preprint arXiv:2107.02314*, 2021. [5](#), [17](#)
- [8] Spyridon Bakas, Hamed Akbari, Aristeidis Sotiras, Michel Bilello, Martin Rozycki, Justin S Kirby, John B Freymann, Keyvan Farahani, and Christos Davatzikos. Advancing the cancer genome atlas glioma mri collections with expert segmentation labels and radiomic features. *Scientific data*, 4(1):1–13, 2017. [17](#)
- [9] Ivana Balažević and et al. Towards in-context scene understanding. *arXiv preprint arXiv:2306.01667*, 2023. [2](#)
- [10] Sophia Bano, Francisco Vasconcelos, Luke M Shepherd, Emmanuel Vander Poorten, Tom Vercauteren, Sébastien Ourselin, Anna L David, Jan Deprest, and Danail Stoyanov. Deep placental vessel segmentation for fetoscopic mosaicking. In *Medical Image Computing and Computer Assisted Intervention–MICCAI 2020: 23rd International Conference, Lima, Peru, October 4–8, 2020, Proceedings, Part III* 23, pages 763–773. Springer, 2020. [17](#)
- [11] Christian F Baumgartner, Kerem C Tezcan, Krishna Chaitanya, Andreas M Hötker, Urs J Muehlematter, Khoschy

- Schawkat, Anton S Becker, Olivio Donati, and Ender Konukoglu. Phiseg: Capturing uncertainty in medical image segmentation. In *Medical Image Computing and Computer Assisted Intervention–MICCAI 2019: 22nd International Conference, Shenzhen, China, October 13–17, 2019, Proceedings, Part II* 22, pages 119–127. Springer, 2019. 2, 5, 6
- [12] Anton S Becker, Krishna Chaitanya, Khoschy Schawkat, Urs J Muehlematter, Andreas M Hötker, Ender Konukoglu, and Olivio F Donati. Variability of manual segmentation of the prostate in axial t2-weighted mri: a multi-reader study. *European journal of radiology*, 121:108716, 2019. 2
- [13] Marc G Bellemare, Ivo Danihelka, Will Dabney, Shakir Mohamed, Balaji Lakshminarayanan, Stephan Hoyer, and Rémi Munos. The cramer distance as a solution to biased wasserstein gradients. *arXiv preprint arXiv:1705.10743*, 2017. 5
- [14] Olivier Bernard, Alain Lalande, Clement Zotti, Frederick Cervenansky, Xin Yang, Pheng-Ann Heng, Irem Cetin, Karim Lekadir, Oscar Camara, Miguel Angel Gonzalez Ballester, et al. Deep learning techniques for automatic mri cardiac multi-structures segmentation and diagnosis: is the problem solved? *IEEE transactions on medical imaging*, 37(11):2514–2525, 2018. 5, 17
- [15] Ishaan Bhat, Josien PW Pluim, and Hugo J Kuijf. Generalized probabilistic u-net for medical image segementation. In *International Workshop on Uncertainty for Safe Utilization of Machine Learning in Medical Imaging*, pages 113–124. Springer, 2022. 2
- [16] Patrick Bilic, Patrick Ferdinand Christ, Eugene Vorontsov, Grzegorz Chlebus, Hao Chen, Qi Dou, Chi-Wing Fu, Xiao Han, Pheng-Ann Heng, Jürgen Hesser, et al. The liver tumor segmentation benchmark (lits). *arXiv preprint arXiv:1901.04056*, 2019. 5, 17
- [17] Nicholas Bloch, Anant Madabhushi, Henkjan Huisman, John Freymann, Justin Kirby, Michael Grauer, Andinet Enquobahrie, Carl Jaffe, Larry Clarke, and Keyvan Farahani. Nci-isbi 2013 challenge: automated segmentation of prostate structures. *The Cancer Imaging Archive*, 370(6):5, 2015. 5, 17
- [18] Mateusz Buda, Ashirbani Saha, and Maciej A Mazurowski. Association of genomic subtypes of lower-grade gliomas with shape features automatically extracted by a deep learning algorithm. *Computers in biology and medicine*, 109: 218–225, 2019. 17
- [19] Victor Ion Butoi, Jose Javier Gonzalez Ortiz, Tianyu Ma, Mert R Sabuncu, John Guttag, and Adrian V Dalca. Universeg: Universal medical image segmentation. *arXiv preprint arXiv:2304.06131*, 2023. 2, 3, 4, 5, 6, 7, 1
- [20] Juan C. Caicedo, Allen Goodman, Kyle W. Karhohs, Beth A. Cimini, Jeanelle Ackerman, Marzieh Haghghi, CherKeng Heng, Tim Becker, Minh Doan, Claire McQuin, Mohammad Rohban, Shantanu Singh, and Anne E. Carpenter. Nucleus segmentation across imaging experiments: the 2018 Data Science Bowl. *Nature Methods*, 16(12):1247–1253, 2019. 17
- [21] Albert Cardon, Stephan Saalfeld, Stephan Preibisch, Benjamin Schmid, Anchi Cheng, Jim Pulkas, Pavel Toman- cak, and Volker Hartenstein. Isbi challenge: Segmentation of neuronal structures in em stacks. 5
- [22] Guillaume Charpiat, Matthias Hofmann, and Bernhard Schölkopf. Automatic image colorization via multimodal predictions. In *Computer Vision–ECCV 2008: 10th European Conference on Computer Vision, Marseille, France, October 12–18, 2008, Proceedings, Part III* 10, pages 126–139. Springer, 2008. 4
- [23] Junlong Cheng, Jin Ye, Zhongying Deng, Jianpin Chen, Tianbin Li, Haoyu Wang, Yanzhou Su, Ziyan Huang, Jilong Chen, Lei Jiang, Hui Sun, Junjun He, Shaoting Zhang, Min Zhu, and Yu Qiao. SAM-Med2D, 2023. arXiv:2308.16184 [cs]. 6
- [24] Noel C. F. Codella, David A. Gutman, M. Emre Celebi, Brian Helba, Michael A. Marchetti, Stephen W. Dusza, Aadi Kalloo, Konstantinos Liopyris, Nabin K. Mishra, Harald Kittler, and Allan Halpern. Skin lesion analysis toward melanoma detection: A challenge at the 2017 international symposium on biomedical imaging (isbi), hosted by the international skin imaging collaboration (ISIC). *CoRR*, abs/1710.05006, 2017. 5
- [25] Seffi Cohen, Niv Goldshlager, Lior Rokach, and Bracha Shapira. Boosting anomaly detection using unsupervised diverse test-time augmentation. *Information Sciences*, 626: 821–836, 2023. 3
- [26] Steffen Czolbe, Kasra Arnavaz, Oswin Krause, and Aasa Feragen. Is segmentation uncertainty useful? In *Information Processing in Medical Imaging: 27th International Conference, IPMI 2021, Virtual Event, June 28–June 30, 2021, Proceedings* 27, pages 715–726. Springer, 2021. 2
- [27] Etienne Decenciere, Guy Cazuguel, Xiwei Zhang, Guillaume Thibault, J-C Klein, Fernand Meyer, Beatriz Martocgui, Gwénolé Quellec, Mathieu Lamard, Roman Danno, et al. Teleophtha: Machine learning and image processing methods for teleophthalmology. *Irbm*, 34(2):196–203, 2013. 17
- [28] Aysen Degerli, Morteza Zabihi, Serkan Kiranyaz, Tahir Hamid, Rashid Mazhar, Ridha Hamila, and Moncef Gabouj. Early detection of myocardial infarction in low-quality echocardiography. *IEEE Access*, 9:34442–34453, 2021. 17
- [29] Armen Der Kiureghian and Ove Ditlevsen. Aleatory or epistemic? does it matter? *Structural safety*, 31(2):105–112, 2009. 2
- [30] Lee R Dice. Measures of the amount of ecologic association between species. *Ecology*, 26(3):297–302, 1945. 5
- [31] Hao Ding, Changchang Sun, Hao Tang, Dawen Cai, and Yan Yan. Few-shot medical image segmentation with cycle-resemblance attention. In *Proceedings of the IEEE/CVF Winter Conference on Applications of Computer Vision*, pages 2488–2497, 2023. 2
- [32] Chelsea Finn, Pieter Abbeel, and Sergey Levine. Model-agnostic meta-learning for fast adaptation of deep networks. In *International conference on machine learning*, pages 1126–1135. PMLR, 2017. 2
- [33] Mélanie Gaillochet, Christian Desrosiers, and Hervé Lombaert. Taal: Test-time augmentation for active learning

- in medical image segmentation. In *Data Augmentation, Labelling, and Imperfections*. Springer Nature Switzerland, 2022. 3
- [34] J Gamper, NA Koohbanani, K Benes, S Graham, M Jahanifar, SA Khurram, A Azam, K Hewitt, and N Rajpoot. Pan-nuke dataset extension, insights and baselines. arxiv. 2020 doi: 10.48550. ARXIV, 2003. 5
- [35] Stephan Gerhard, Jan Funke, Julien Martel, Albert Cardona, and Richard Fetter. Segmented anisotropic ssTEM dataset of neural tissue. *figshare*, pages 0–0, 2013.
- [36] Randy L Gollub, Jody M Shoemaker, Margaret D King, Tonya White, Stefan Ehrlich, Scott R Sponheim, Vincent P Clark, Jessica A Turner, Bryon A Mueller, Vince Magnotta, et al. The mcic collection: a shared repository of multi-modal, multi-site brain image data from a clinical investigation of schizophrenia. *Neuroinformatics*, 11:367–388, 2013. 5, 17
- [37] Ioannis S Gousias, Daniel Rueckert, Rolf A Heckemann, Leigh E Dyet, James P Boardman, A David Edwards, and Alexander Hammers. Automatic segmentation of brain mris of 2-year-olds into 83 regions of interest. *Neuroimage*, 40(2):672–684, 2008. 17
- [38] Ioannis S Gousias, A David Edwards, Mary A Rutherford, Serena J Counsell, Jo V Hajnal, Daniel Rueckert, and Alexander Hammers. Magnetic resonance imaging of the newborn brain: manual segmentation of labelled atlases in term-born and preterm infants. *Neuroimage*, 62(3):1499–1509, 2012. 17
- [39] Simon Graham, Quoc Dang Vu, Shan E Ahmed Raza, Ayesha Azam, Yee Wah Tsang, Jin Tae Kwak, and Nasir Rajpoot. Hover-net: Simultaneous segmentation and classification of nuclei in multi-tissue histology images. *Medical Image Analysis*, 58:101563, 2019. 5
- [40] Daniel Gut. X-ray images of the hip joints. 1, 2021. Publisher: Mendeley Data. 5, 17
- [41] Abner Guzman-Rivera, Dhruv Batra, and Pushmeet Kohli. Multiple choice learning: Learning to produce multiple structured outputs. *Advances in neural information processing systems*, 25, 2012. 4
- [42] Nicholas Heller, Fabian Isensee, Klaus H Maier-Hein, Xiaoshuai Hou, Chunmei Xie, Fengyi Li, Yang Nan, Guangrui Mu, Zhiyong Lin, Miofei Han, et al. The state of the art in kidney and kidney tumor segmentation in contrast-enhanced ct imaging: Results of the kits19 challenge. *Medical Image Analysis*, page 101821, 2020. 5, 17
- [43] Moritz R Hernandez Petzsche, Ezequiel de la Rosa, Uta Hanning, Roland Wiest, Waldo Valenzuela, Mauricio Reyes, Maria Meyer, Sook-Lei Liew, Florian Kofler, Ivan Ezhov, et al. Isles 2022: A multi-center magnetic resonance imaging stroke lesion segmentation dataset. *Scientific data*, 9(1):762, 2022. 5, 17
- [44] Malte Hoffmann, Benjamin Billot, Douglas N Greve, Juan Eugenio Iglesias, Bruce Fischl, and Adrian V Dalca. Synthmorph: learning contrast-invariant registration without acquired images. *IEEE transactions on medical imaging*, 41(3):543–558, 2021. 5
- [45] Sungmin Hong, Anna K Bonkhoff, Andrew Hoopes, Martin Bretzner, Markus D Schirmer, Anne-Katrin Giese, Adrian V Dalca, Polina Golland, and Natalia S Rost. Hypernet-ensemble learning of segmentation probability for medical image segmentation with ambiguous labels. *arXiv preprint arXiv:2112.06693*, 2021. 2
- [46] Andrew Hoopes, Malte Hoffmann, Douglas N. Greve, Bruce Fischl, John Guttag, and Adrian V. Dalca. Learning the effect of registration hyperparameters with hypermorph. pages 1–30, 2022. 17
- [47] AD Hoover, Valentina Kouznetsova, and Michael Goldbaum. Locating blood vessels in retinal images by piecewise threshold probing of a matched filter response. *IEEE Transactions on Medical imaging*, 19(3):203–210, 2000. 5, 18
- [48] Qingqiao Hu, Hao Wang, Jing Luo, Yunhao Luo, Zhi-heng Zhang, Jan S Kirschke, Benedikt Wiestler, Bjoern Menze, Jianguo Zhang, and Hongwei Bran Li. Inter-rater uncertainty quantification in medical image segmentation via rater-specific bayesian neural networks. *arXiv preprint arXiv:2306.16556*, 2023. 2
- [49] Xiaoqiong Huang, Zejian Chen, Xin Yang, Zhendong Liu, Yuxin Zou, Mingyuan Luo, Wufeng Xue, and Dong Ni. Style-invariant cardiac image segmentation with test-time augmentation. In *Statistical Atlases and Computational Models of the Heart. M&Ms and EMIDEC Challenges: 11th International Workshop, STACOM 2020, Held in Conjunction with MICCAI 2020, Lima, Peru, October 4, 2020, Revised Selected Papers 11*, pages 305–315. Springer, 2021. 3
- [50] Humans in the Loop. Teeth segmentation dataset. 5, 17
- [51] Fabian Isensee, Paul F Jaeger, Simon AA Kohl, Jens Petersen, and Klaus H Maier-Hein. nnunet: a self-configuring method for deep learning-based biomedical image segmentation. *Nature methods*, 18(2):203–211, 2021. 2
- [52] Mobarakol Islam and Ben Glocker. Spatially varying label smoothing: Capturing uncertainty from expert annotations. In *Information Processing in Medical Imaging: 27th International Conference, IPMI 2021, Virtual Event, June 28–June 30, 2021, Proceedings 27*, pages 677–688. Springer, 2021. 2
- [53] Debesh Jha, Pia H Smedsrød, Dag Johansen, Thomas de Lange, Håvard D Johansen, Pål Halvorsen, and Michael A Riegler. A comprehensive study on colorectal polyp segmentation with resunet++, conditional random field and test-time augmentation. *IEEE journal of biomedical and health informatics*, 25(6):2029–2040, 2021. 3
- [54] Yuanfeng Ji, Haotian Bai, Jie Yang, Chongjian Ge, Ye Zhu, Ruimao Zhang, Zhen Li, Lingyan Zhang, Wanling Ma, Xi-ang Wan, et al. Amos: A large-scale abdominal multi-organ benchmark for versatile medical image segmentation. *arXiv preprint arXiv:2206.08023*, 2022. 5, 17
- [55] Leo Joskowicz, D Cohen, N Caplan, and Jacob Sosna. Inter-observer variability of manual contour delineation of structures in ct. *European radiology*, 29:1391–1399, 2019. 2
- [56] Rashed Karim, R James Housden, Mayuragoban Balasubramaniam, Zhong Chen, Daniel Perry, Ayesha Uddin, Yosra

- Al-Beyatti, Ebrahim Palkhi, Prince Acheampong, Samantha Obom, et al. Evaluation of current algorithms for segmentation of scar tissue from late gadolinium enhancement cardiovascular magnetic resonance of the left atrium: an open-access grand challenge. *Journal of Cardiovascular Magnetic Resonance*, 15(1):1–17, 2013. [5](#), [17](#)
- [57] Ali Emre Kavur, M. Alper Selver, Oğuz Dicle, Mustafa Barış, and N. Sinem Gezer. CHAOS - Combined (CT-MR) Healthy Abdominal Organ Segmentation Challenge Data. 2019. [5](#)
- [58] Ali Emre Kavur, M. Alper Selver, Oğuz Dicle, Mustafa Barış, and N. Sinem Gezer. CHAOS - Combined (CT-MR) Healthy Abdominal Organ Segmentation Challenge Data, 2019. [17](#)
- [59] A. Emre Kavur, N. Sinem Gezer, Mustafa Barış, Sinem Aslan, Pierre-Henri Conze, Vladimir Groza, Duc Duy Pham, Soumick Chatterjee, Philipp Ernst, Savaş Özkan, Bora Baydar, Dmitry Lachinov, Shuo Han, Josef Pauli, Fabian Isensee, Matthias Perkonigg, Rachana Sathish, Ronnie Rajan, Debdoot Sheet, Gurbandurdy Dovletov, Oliver Speck, Andreas Nürnberger, Klaus H. Maier-Hein, Gözde Bozdağı Akar, Gözde Ünal, Oğuz Dicle, and M. Alper Selver. CHAOS Challenge - combined (CT-MR) healthy abdominal organ segmentation. *Medical Image Analysis*, 69:101950, 2021. [5](#)
- [60] A. Emre Kavur, N. Sinem Gezer, Mustafa Barış, Sinem Aslan, Pierre-Henri Conze, Vladimir Groza, Duc Duy Pham, Soumick Chatterjee, Philipp Ernst, Savaş Özkan, Bora Baydar, Dmitry Lachinov, Shuo Han, Josef Pauli, Fabian Isensee, Matthias Perkonigg, Rachana Sathish, Ronnie Rajan, Debdoot Sheet, Gurbandurdy Dovletov, Oliver Speck, Andreas Nürnberger, Klaus H. Maier-Hein, Gözde Bozdağı Akar, Gözde Ünal, Oğuz Dicle, and M. Alper Selver. CHAOS Challenge - combined (CT-MR) healthy abdominal organ segmentation. *Medical Image Analysis*, 69:101950, 2021. [17](#)
- [61] Alex Kendall and Yarin Gal. What uncertainties do we need in bayesian deep learning for computer vision? *Advances in neural information processing systems*, 30, 2017. [2](#)
- [62] Alex Kendall, Vijay Badrinarayanan, and Roberto Cipolla. Bayesian segnet: Model uncertainty in deep convolutional encoder-decoder architectures for scene understanding. *arXiv preprint arXiv:1511.02680*, 2015. [2](#)
- [63] Dongyun Kim, Jinwoo Kim, Seongwoong Cho, Chong Luo, and Seunghoon Hong. Universal few-shot learning of dense prediction tasks with visual token matching. *arXiv preprint arXiv:2303.14969*, 2023. [2](#)
- [64] Kwanyoung Kim, Dongwon Park, Kwang In Kim, and Se Young Chun. Task-aware variational adversarial active learning. In *Proceedings of the IEEE/CVF Conference on Computer Vision and Pattern Recognition*, pages 8166–8175, 2021. [3](#)
- [65] Serkan Kiranyaz, Aysen Degerli, Tahir Hamid, Rashid Mazhar, Rayyan El Fadil Ahmed, Rayaan Abouhasera, Morteza Zabihi, Junaid Malik, Ridha Hamila, and Moncef Gabbouj. Left ventricular wall motion estimation by active polynomials for acute myocardial infarction detection. *IEEE Access*, 8:210301–210317, 2020. [17](#)
- [66] Alexander Kirillov and et al. Segment anything. *arXiv preprint arXiv:2304.02643*, 2023. [4](#), [6](#)
- [67] Simon Kohl, Bernardino Romera-Paredes, Clemens Meyer, Jeffrey De Fauw, Joseph R Ledsam, Klaus Maier-Hein, SM Eslami, Danilo Jimenez Rezende, and Olaf Ronneberger. A probabilistic u-net for segmentation of ambiguous images. *Advances in neural information processing systems*, 31, 2018. [2](#), [5](#), [6](#)
- [68] Simon AA Kohl, Bernardino Romera-Paredes, Klaus H Maier-Hein, Danilo Jimenez Rezende, SM Eslami, Pushmeet Kohli, Andrew Zisserman, and Olaf Ronneberger. A hierarchical probabilistic u-net for modeling multi-scale ambiguities. *arXiv preprint arXiv:1905.13077*, 2019. [2](#), [8](#)
- [69] Markus Krönke, Christine Eilers, Desislava Dimova, Melanie Köhler, Gabriel Buschner, Lilit Schweiger, Lemonia Konstantinidou, Marcus Makowski, James Nagarajah, Nassir Navab, et al. Tracked 3d ultrasound and deep neural network-based thyroid segmentation reduce interobserver variability in thyroid volumetry. *Plos one*, 17(7):e0268550, 2022. [5](#)
- [70] Harold W Kuhn. The hungarian method for the assignment problem. *Naval research logistics quarterly*, 2(1-2):83–97, 1955. [8](#)
- [71] Hugo J Kuijf, J Matthijs Biesbroek, Jeroen De Bresser, Rutger Heinen, Simon Andermatt, Mariana Bento, Matt Berseth, Mikhail Belyaev, M Jorge Cardoso, Adria Casamitjana, et al. Standardized assessment of automatic segmentation of white matter hyperintensities and results of the wmh segmentation challenge. *IEEE transactions on medical imaging*, 38(11):2556–2568, 2019. [5](#), [17](#)
- [72] Maria Kuklisova-Murgasova, Paul Aljabar, Latha Srinivasan, Serena J Counsell, Valentina Doria, Ahmed Serag, Ioannis S Gousias, James P Boardman, Mary A Rutherford, A David Edwards, et al. A dynamic 4d probabilistic atlas of the developing brain. *NeuroImage*, 54(4):2750–2763, 2011. [5](#), [17](#)
- [73] Benjamin Lambert, Florence Forbes, Senan Doyle, and Michel Dojat. Triadnet: Sampling-free predictive intervals for lesional volume in 3d brain mr images. In *Uncertainty for Safe Utilization of Machine Learning in Medical Imaging – MICCAI 2023*. Springer Nature Switzerland, 2023. [2](#)
- [74] Zoé Lambert, Caroline Petitjean, Bernard Dubray, and Su Kuan. Segthor: segmentation of thoracic organs at risk in ct images. In *2020 Tenth International Conference on Image Processing Theory, Tools and Applications (IPTA)*, pages 1–6. IEEE, 2020. [5](#), [17](#)
- [75] Bennett Landman, Zhoubing Xu, J Igelsias, Martin Styner, T Langerak, and Arno Klein. Miccai multi-atlas labeling beyond the cranial vault–workshop and challenge. In *Proc. MICCAI Multi-Atlas Labeling Beyond Cranial Vault—Workshop Challenge*, page 12, 2015. [5](#), [17](#)
- [76] Agostina Larrazabal, Cesar Martinez, Jose Dolz, and Enzo Ferrante. Maximum entropy on erroneous predictions (meep): Improving model calibration for medical image segmentation. *arXiv preprint arXiv:2112.12218*, 2021. [2](#)
- [77] Sarah Leclerc, Erik Smistad, Joao Pedrosa, Andreas Østvik, Frederic Cervenansky, Florian Espinosa, Torvald Espeland,

- Erik Andreas Rye Berg, Pierre-Marc Jodoin, Thomas Grenier, et al. Deep learning for segmentation using an open large-scale dataset in 2d echocardiography. *IEEE transactions on medical imaging*, 38(9):2198–2210, 2019. [5](#), [17](#)
- [78] Guillaume Lemaître, Robert Martí, Jordi Freixenet, Joan C Vilanova, Paul M Walker, and Fabrice Meriaudeau. Computer-aided detection and diagnosis for prostate cancer based on mono and multi-parametric mri: a review. *Computers in biology and medicine*, 60:8–31, 2015. [17](#)
- [79] Mingchao Li, Yuhan Zhang, Zexuan Ji, Keren Xie, Songtao Yuan, Qinghuai Liu, and Qiang Chen. Ipn-v2 and octa-500: Methodology and dataset for retinal image segmentation. *arXiv preprint arXiv:2012.07261*, 2020. [5](#), [17](#)
- [80] Yiwen Li, Yunguan Fu, Iani Gayo, Qianye Yang, Zhe Min, Shaheer Saeed, Wen Yan, Yipei Wang, J Alison Noble, Mark Emberton, et al. Prototypical few-shot segmentation for cross-institution male pelvic structures with spatial registration. *arXiv preprint arXiv:2209.05160*, 2022. [2](#)
- [81] Zhuwen Li, Qifeng Chen, and Vladlen Koltun. Interactive image segmentation with latent diversity. In *Proceedings of the IEEE Conference on Computer Vision and Pattern Recognition*, pages 577–585, 2018. [4](#)
- [82] Geert Litjens, Robert Toth, Wendy van de Ven, Caroline Hoeks, Sjoerd Kerkstra, Bram van Ginneken, Graham Vincent, Gwenael Guillard, Neil Birbeck, Jindang Zhang, et al. Evaluation of prostate segmentation algorithms for mri: the promise12 challenge. *Medical image analysis*, 18(2):359–373, 2014. [5](#), [17](#)
- [83] Vebjorn Ljosa, Katherine L Sokolnicki, and Anne E Carpenter. Annotated high-throughput microscopy image sets for validation. *Nature methods*, 9(7):637–637, 2012. [17](#)
- [84] Maximilian T Löffler, Anjany Sekuboyina, Alina Jacob, Anna-Lena Grau, Andreas Scharr, Malek El Husseini, Mareike Kallweit, Claus Zimmer, Thomas Baum, and Jan S Kirschke. A vertebral segmentation dataset with fracture grading. *Radiology: Artificial Intelligence*, 2(4):e190138, 2020.
- [85] Xiangde Luo, Wenjun Liao, Jianghong Xiao, Tao Song, Xiaofan Zhang, Kang Li, Guotai Wang, and Shaoting Zhang. Word: Revisiting organs segmentation in the whole abdominal region. *arXiv preprint arXiv:2111.02403*, 2021. [17](#)
- [86] Yuhui Ma, Huaying Hao, Jianyang Xie, Huazhu Fu, Jiong Zhang, Jianlong Yang, Zhen Wang, Jiang Liu, Yalin Zheng, and Yitian Zhao. Rose: a retinal oct-angiography vessel segmentation dataset and new model. *IEEE Transactions on Medical Imaging*, 40(3):928–939, 2021. [17](#)
- [87] Jacob A. Macdonald, Zhe Zhu, Brandon Konkel, Maciej Mazurowski, Walter Wiggins, and Mustafa Bashir. Duke liver dataset (MRI) v2, 2023.
- [88] Daniel S Marcus, Tracy H Wang, Jamie Parker, John G Csernansky, John C Morris, and Randy L Buckner. Open access series of imaging studies (oasis): cross-sectional mri data in young, middle aged, nondemented, and demented older adults. *Journal of cognitive neuroscience*, 19(9):1498–1507, 2007. [17](#)
- [89] Kenneth Marek, Danna Jennings, Shirley Lasch, Andrew Siderowf, Caroline Tanner, Tanya Simuni, Chris Coffey, Karl Kieburtz, Emily Flagg, Sohini Chowdhury, et al. The parkinson progression marker initiative (ppmi). *Progress in neurobiology*, 95(4):629–635, 2011. [5](#), [17](#)
- [90] Kazuhisa Matsunaga, Akira Hamada, Akane Minagawa, and Hiroshi Koga. Image classification of melanoma, nevus and seborrheic keratosis by deep neural network ensemble. *arXiv preprint arXiv:1703.03108*, 2017. [3](#)
- [91] Maciej A Mazurowski, Kal Clark, Nicholas M Czarnek, Parisa Shamsesfandabadi, Katherine B Peters, and Ashirbani Saha. Radiogenomics of lower-grade glioma: algorithmically-assessed tumor shape is associated with tumor genomic subtypes and patient outcomes in a multi-institutional study with the cancer genome atlas data. *Journal of neuro-oncology*, 133:27–35, 2017. [5](#), [17](#)
- [92] Bjoern Menze, Leo Joskowicz, Spyridon Bakas, Andras Jakab, Ender Konukoglu, Anton Becker, Amber Simpson, and Richard D. Quantification of uncertainties in biomedical image quantification 2021. *4th International Conference on Medical Image Computing and Computer Assisted Intervention (MICCAI 2021)*, 2021. [5](#), [18](#)
- [93] Bjoern H Menze, Andras Jakab, Stefan Bauer, Jayashree Kalpathy-Cramer, Keyvan Farahani, Justin Kirby, Yuliya Burren, Nicole Porz, Johannes Slotboom, Roland Wiest, et al. The multimodal brain tumor image segmentation benchmark (brats). *IEEE transactions on medical imaging*, 34(10):1993–2024, 2014. [17](#)
- [94] Fausto Milletari, Nassir Navab, and Seyed-Ahmad Ahmadi. V-net: Fully convolutional neural networks for volumetric medical image segmentation. In *2016 fourth international conference on 3D vision (3DV)*, pages 565–571. Ieee, 2016. [4](#)
- [95] Miguel Monteiro, Loïc Le Folgoc, Daniel Coelho de Castro, Nick Pawlowski, Bernardo Marques, Konstantinos Kamnitsas, Mark van der Wilk, and Ben Glocker. Stochastic segmentation networks: Modelling spatially correlated aleatoric uncertainty. *Advances in Neural Information Processing Systems*, 33:12756–12767, 2020. [2](#), [5](#), [8](#)
- [96] Anna Montoya, Hasnin, kaggle446, shirzad, Will Cukierski, and yffud. Ultrasound nerve segmentation, 2016. [5](#)
- [97] Nikita Moshkov, Botond Mathe, Attila Kertesz-Farkas, Reka Hollandi, and Peter Horvath. Test-time augmentation for deep learning-based cell segmentation on microscopy images. *Scientific reports*, 10(1):5068, 2020. [3](#)
- [98] Khoi Nguyen and Sinisa Todorovic. Feature weighting and boosting for few-shot segmentation. In *Proceedings of the IEEE/CVF International Conference on Computer Vision*, pages 622–631, 2019. [2](#)
- [99] Alex Nichol, Joshua Achiam, and John Schulman. On first-order meta-learning algorithms. *arXiv preprint arXiv:1803.02999*, 2018. [2](#)
- [100] Brennan Nichyporuk, Jillian Cardinell, Justin Szeto, Raghav Mehta, Jean-Pierre R Falet, Douglas L Arnold, Sotirios A Tsaftaris, and Tal Arbel. Rethinking generalization: The impact of annotation style on medical image segmentation. *arXiv preprint arXiv:2210.17398*, 2022. [2](#)
- [101] Prashant Pandey, Mustafa Chasmai, Tanuj Sur, and Brejesh Lall. Robust prototypical few-shot organ segmentation

- with regularized neural-odes. *IEEE Transactions on Medical Imaging*, 2023. 2
- [102] Kelly Payette, Priscille de Dumast, Hamza Kebiri, Ivan Ezhov, Johannes C Paetzold, Suprosanna Shit, Asim Iqbal, Romesa Khan, Raimund Kottke, Patrice Grethen, et al. An automatic multi-tissue human fetal brain segmentation benchmark using the fetal tissue annotation dataset. *Scientific Data*, 8(1):1–14, 2021. 17
- [103] Prasanna Porwal, Samiksha Pachade, Ravi Kamble, Manesh Kokare, Girish Deshmukh, Vivek Sahasrabuddhe, and Fabrice Meriaudeau. Indian diabetic retinopathy image dataset (idrid), 2018. 5, 17
- [104] Perry Radau, Yingli Lu, Kim Connelly, Gideon Paul, AJWG Dick, and Graham Wright. Evaluation framework for algorithms segmenting short axis cardiac mri. *The MIDAS Journal-Cardiac MR Left Ventricle Segmentation Challenge*, 49, 2009. 5, 17
- [105] Aimon Rahman, Jeya Maria Jose Valanarasu, Ilker Haci-haliloglu, and Vishal M Patel. Ambiguous medical image segmentation using diffusion models. In *Proceedings of the IEEE/CVF Conference on Computer Vision and Pattern Recognition*, pages 11536–11546, 2023. 2, 5, 6
- [106] Blaine Rister, Darvin Yi, Kaushik Shivakumar, Tomomi Nobashi, and Daniel L. Rubin. CT-ORG, a new dataset for multiple organ segmentation in computed tomography. *Scientific Data*, 7(1):381, 2020. 5, 17
- [107] Olaf Ronneberger, Philipp Fischer, and Thomas Brox. U-Net: Convolutional Networks for Biomedical Image Segmentation. In *Medical Image Computing and Computer Assisted Intervention – MICCAI 2015*. Springer International Publishing, 2015. 2, 3
- [108] Abhijit Guha Roy, Shayan Siddiqui, Sebastian Pölsterl, Nassir Navab, and Christian Wachinger. Squeeze & excite guided few-shot segmentation of volumetric images. *Medical image analysis*, 59:101587, 2020. 6
- [109] Tim Salimans, Han Zhang, Alec Radford, and Dimitris Metaxas. Improving gans using optimal transport. *arXiv preprint arXiv:1803.05573*, 2018. 5
- [110] Adriel Saporta, Xiaotong Gui, Ashwin Agrawal, Anuj Parereek, SQ Truong, CD Nguyen, Van-Doan Ngo, Jayne Seekins, Francis G Blankenberg, AY Ng, et al. Deep learning saliency maps do not accurately highlight diagnostically relevant regions for medical image interpretation. *MedRxiv*, 2021. 5, 17
- [111] Arne Schmidt, Pablo Morales-Álvarez, and Rafael Molina. Probabilistic modeling of inter-and intra-observer variability in medical image segmentation. In *Proceedings of the IEEE/CVF International Conference on Computer Vision*, pages 21097–21106, 2023. 2
- [112] Constantin Seibold, Simon Reiß, Saquib Sarfraz, Matthias A. Fink, Victoria Mayer, Jan Sellner, Moon Sung Kim, Klaus H. Maier-Hein, Jens Kleesiek, and Rainer Stiefelhagen. Detailed annotations of chest x-rays via ct projection for report understanding. In *Proceedings of the 33th British Machine Vision Conference (BMVC)*, 2022. 5, 17
- [113] Jun Seo, Young-Hyun Park, Sung Whan Yoon, and Jaekyun Moon. Task-adaptive feature transformer with semantic enrichment for few-shot segmentation. *arXiv preprint arXiv:2202.06498*, 2022. 2
- [114] Ahmed Serag, Paul Aljabar, Gareth Ball, Serena J Counsell, James P Boardman, Mary A Rutherford, A David Edwards, Joseph V Hajnal, and Daniel Rueckert. Construction of a consistent high-definition spatio-temporal atlas of the developing brain using adaptive kernel regression. *Neuroimage*, 59(3):2255–2265, 2012. 17
- [115] Arnaud Arindra Adiyoso Setio, Alberto Traverso, Thomas De Bel, Moira SN Berens, Cas Van Den Bogaard, Piergiorgio Cerello, Hao Chen, Qi Dou, Maria Evelina Fantacci, Bram Geurts, et al. Validation, comparison, and combination of algorithms for automatic detection of pulmonary nodules in computed tomography images: the luna16 challenge. *Medical image analysis*, 42:1–13, 2017. 5, 17
- [116] Divya Shanmugam, Davis Blalock, Guha Balakrishnan, and John Guttag. Better aggregation in test-time augmentation. In *Proceedings of the IEEE/CVF international conference on computer vision*, pages 1214–1223, 2021. 3
- [117] Qianqian Shen, Yanan Li, Jiyong Jin, and Bin Liu. Q-net: Query-informed few-shot medical image segmentation. *arXiv preprint arXiv:2208.11451*, 2022. 2
- [118] Amber L Simpson, Michela Antonelli, Spyridon Bakas, Michel Bilello, Keyvan Farahani, Bram Van Ginneken, Annette Kopp-Schneider, Bennett A Landman, Geert Litjens, Bjoern Menze, et al. A large annotated medical image dataset for the development and evaluation of segmentation algorithms. *arXiv preprint arXiv:1902.09063*, 2019. 5, 17
- [119] Samarth Sinha, Sayna Ebrahimi, and Trevor Darrell. Variational adversarial active learning. In *Proceedings of the IEEE/CVF International Conference on Computer Vision*, pages 5972–5981, 2019. 3
- [120] Jake Snell, Kevin Swersky, and Richard Zemel. Prototypical networks for few-shot learning. *Advances in neural information processing systems*, 30, 2017. 2
- [121] Yuxin Song, Jing Zheng, Long Lei, Zhipeng Ni, Baoliang Zhao, and Ying Hu. CT2US: Cross-modal transfer learning for kidney segmentation in ultrasound images with synthesized data. *Ultrasonics*, 122:106706, 2022. 5
- [122] Joes Staal, Michael D Abràmoff, Meindert Niemeijer, Max A Viergever, and Bram Van Ginneken. Ridge-based vessel segmentation in color images of the retina. *IEEE transactions on medical imaging*, 23(4):501–509, 2004. 5, 17
- [123] Gábor J Székely and Maria L Rizzo. Energy statistics: A class of statistics based on distances. *Journal of statistical planning and inference*, 143(8):1249–1272, 2013. 5
- [124] Ryutaro Tanno, Ardavan Saeedi, Swami Sankaranarayanan, Daniel C Alexander, and Nathan Silberman. Learning from noisy labels by regularized estimation of annotator confusion. In *Proceedings of the IEEE/CVF conference on computer vision and pattern recognition*, pages 11244–11253, 2019. 2
- [125] Oriol Vinyals, Charles Blundell, Timothy Lillicrap, Daan Wierstra, et al. Matching networks for one shot learning. *Advances in neural information processing systems*, 29, 2016. 2

- [126] Guotai Wang, Wenqi Li, Michael Aertsen, Jan Deprest, Sébastien Ourselin, and Tom Vercauteren. Aleatoric uncertainty estimation with test-time augmentation for medical image segmentation with convolutional neural networks. *Neurocomputing*, 338:34–45, 2019. 3
- [127] Guotai Wang, Wenqi Li, Sébastien Ourselin, and Tom Vercauteren. Automatic brain tumor segmentation using convolutional neural networks with test-time augmentation. In *Brainlesion: Glioma, Multiple Sclerosis, Stroke and Traumatic Brain Injuries: 4th International Workshop, BrainLes 2018, Held in Conjunction with MICCAI 2018, Granada, Spain, September 16, 2018, Revised Selected Papers, Part II* 4, pages 61–72. Springer, 2019. 3
- [128] Xinlong Wang, Wen Wang, Yue Cao, Chunhua Shen, and Tiejun Huang. Images speak in images: A generalist painter for in-context visual learning. In *Proceedings of the IEEE/CVF Conference on Computer Vision and Pattern Recognition*, pages 6830–6839, 2023. 2
- [129] Xinlong Wang, Xiaosong Zhang, Yue Cao, Wen Wang, Chunhua Shen, and Tiejun Huang. Seggpt: Towards segmenting everything in context. In *Proceedings of the IEEE/CVF International Conference on Computer Vision*, pages 1130–1140, 2023. 2, 6
- [130] Julia Wolleb, Robin Sandkühler, Florentin Bieder, Philippe Valmaggia, and Philippe C. Cattin. Diffusion Models for Implicit Image Segmentation Ensembles. In *Medical Imaging with Deep Learning*, 2021. 2
- [131] Hallee E Wong, Marianne Rakic, John Guttag, and Adrian V Dalca. Scribbleprompt: Fast and flexible interactive segmentation for any medical image. *arXiv preprint arXiv:2312.07381*, 2023. 5, 1
- [132] Andre Ye, Quan Ze Chen, and Amy Zhang. Confidence contours: Uncertainty-aware annotation for medical semantic segmentation. *arXiv preprint arXiv:2308.07528*, 2023. 2
- [133] Lukas Zbinden, Lars Doorenbos, Theodoros Pissas, Adrian Thomas Huber, Raphael Sznitman, and Pablo Márquez-Neila. Stochastic segmentation with conditional categorical diffusion models. In *Proceedings of the IEEE/CVF International Conference on Computer Vision*, pages 1119–1129, 2023. 2, 5, 8
- [134] Chi Zhang, Guosheng Lin, Fayao Liu, Rui Yao, and Chunhua Shen. Canet: Class-agnostic segmentation networks with iterative refinement and attentive few-shot learning. In *Proceedings of the IEEE/CVF conference on computer vision and pattern recognition*, pages 5217–5226, 2019. 2
- [135] Yingtao Zhang, Min Xian, Heng-Da Cheng, Bryar Shareef, Jianrui Ding, Fei Xu, Kuan Huang, Boyu Zhang, Chunning Ning, and Ying Wang. Busis: A benchmark for breast ultrasound image segmentation. In *Healthcare*, page 729. MDPI, 2022. 5
- [136] Yingtao Zhang, Min Xian, Heng-Da Cheng, Bryar Shareef, Jianrui Ding, Fei Xu, Kuan Huang, Boyu Zhang, Chunning Ning, and Ying Wang. Busis: A benchmark for breast ultrasound image segmentation. In *Healthcare*, page 729. MDPI, 2022. 17
- [137] Qi Zhao, Shuchang Lyu, Wenpei Bai, Linghan Cai, Binghao Liu, Meijing Wu, Xiubo Sang, Min Yang, and Lijiang Chen. A multi-modality ovarian tumor ultrasound image dataset for unsupervised cross-domain semantic segmentation. *CoRR*, abs/2207.06799, 2022. 5
- [138] Guoyan Zheng, Chengwen Chu, Daniel L Belavý, Bulat Ibragimov, Robert Korez, Tomaž Vrtovec, Hugo Hutt, Richard Everson, Judith Meakin, Isabel López Andrade, et al. Evaluation and comparison of 3d intervertebral disc localization and segmentation methods for 3d t2 mr data: A grand challenge. *Medical image analysis*, 35:327–344, 2017. 5, 17
- [139] Xin Zheng, Yong Wang, Guoyou Wang, and Jianguo Liu. Fast and robust segmentation of white blood cell images by self-supervised learning. *Micron*, 107:55–71, 2018. 5, 17

# Tyche: Stochastic In-Context Learning for Medical Image Segmentation

## Supplementary Material

### A. Overview

We first present a brief overview of the analysis and information in this Supplementary Material.

#### Tyche Model Choices.

We present additional data details, including for MegaMedical, multi-annotator data, and simulated data. We give additional details on the *Tyche-TS* training strategy, as well as the augmentations used at inference for *Tyche-IS*. We also detail how we trained each benchmark, and their respective limitations.

We provide an intuition behind the best candidate Dice loss, and show that with *Tyche*, it is possible to optimize for objectives that apply to the candidate predictions as a group, and show results when optimizing GED.

#### Tyche Analysis.

For *Tyche-TS*, we investigate four aspects: noise, context set, number of predictions, and *SetBlock*. We show how different noise levels impact the predictions. Moreover, we give examples of how prediction changes when the context or the noise changes. We also show that the number of predictions at inference impacts the diversity of the segmentation candidates predicted.

For *Tyche-IS*, we investigate how different augmentations affect performance.

We also analyze a scenario where only few of annotated examples are available, using the LIDC-IDRI dataset. We compare *Tyche* with these samples in the context to PhiSeg, trained on these few annotated samples.

#### Further Evaluation.

Given the nature of stochastic segmentation tasks, no single metric fits all purposes, and the optimal metric depends on the downstream goals. We provide *sample diversity* and *Hungarian Matching*, showing that *Tyche* performs well on these as well.

We also present performance per dataset and show that the relative performance of each model stays generally unchanged, even though the difficulty of each dataset is widely different.

We provide additional visualizations on how *Tyche* and the baselines perform for each datasets, both on single and multi-annotator data.

**Data split.** All analysis results in this supplemental material use the validation set of the out-of-distribution datasets, to avoid making modeling decisions on the test sets.

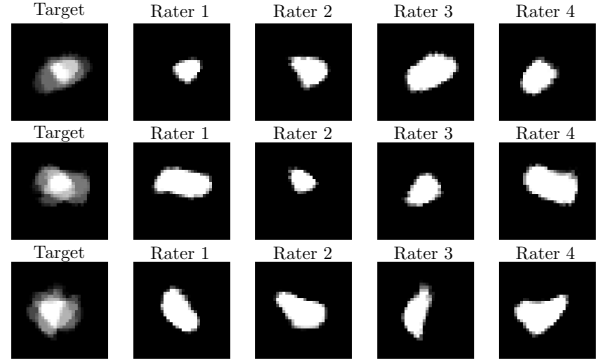


Figure 10. **Synthetic Multi-Annotated Examples.** Each blob is generated by deforming a white disk using a random smooth deformation field, each representing a different rater. The blobs are then averaged to form the target image to segment.

### B. Tyche Model Choices

We present the implementation details for the data, our *Tyche* models, and the benchmarks.

#### B.1. Medical Image Data

**Megamedical.** We build on the dataset collection proposed in [19, 131], using the similar preprocessing methods. The complete list of datasets is presented Table 10.

**Processing.** Each image is normalized between 0 and 1 and is resized to  $128 \times 128$ . When the full 3D volume is available, we take two slices for each task: the slice in the middle of the volume and the slice with the largest count of pixels labelled for that task.

**Task Definition.** We consider a task as labelling a certain structure from a certain modality for a certain dataset. If a given medical image has different structures labeled, we consider each structure a different task. For 3D volumes, we consider each axis a different task.

**Synthetic Data.** We use a set of synthetic tasks to enhance the performance of our networks, similar to [19]. Some examples are shown in Figure 11.

**Synthetic Multi-Annotator Data.** We use synthetic data to encourage diversity in our predictions. Figure 10 shows examples of blob targets with the corresponding simulated annotations.

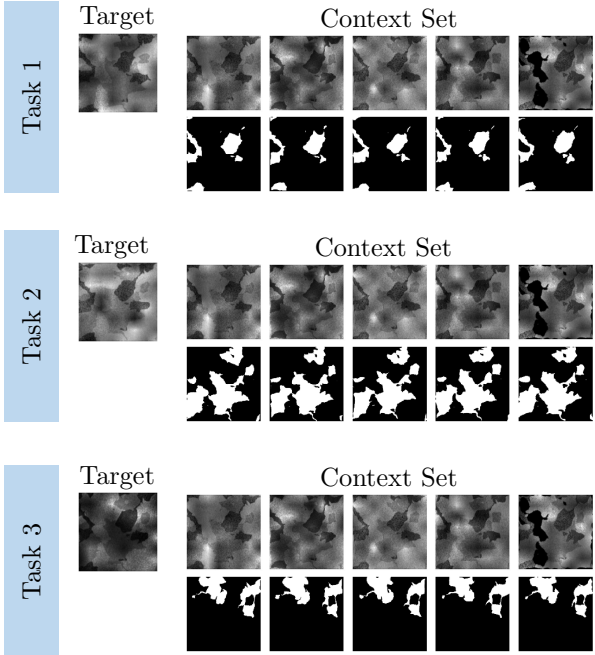


Figure 11. **Synthetic Data Examples.** Example of training images on the single annotator synthetic data. Each row is an example of a target-context pair corresponding to a different task.

## B.2. Training of Tyche-TS

We train *Tyche-TS* with a context size of 16 and a batch size of 4. We use a learning rate of 0.0001, Adam as an optimizer, and a kernel size of 3. We apply the augmentations shown Table 6. To obtain  $K$  segmentation candidates, we generate  $K$  noise samples  $z_k \sim \mathcal{N}(0, \mathbb{I})$ . We duplicate the input  $K$  times and concatenate each noise sample with a duplicated target to form  $K$  stochastic inputs to the network.

## B.3. Network for Tyche-IS

For the *Tyche-IS* network, we use the baseline UniverSeg [19], trained with the same data as *Tyche-TS*, same batch size, and same context size. At test time, we use the augmentations in Table 7. Figure 12 shows example augmentation on different samples.

## B.4. Benchmarks

We distinguish three types of benchmarks: in-context methods, that can take as input a context set, the interactive frameworks, and the task-trained specialized upper bounds.

**In-context baselines.** Because they were trained on medical data, we use SegGPT and SAM-Med2D as provided in their official release. We train from scratch UniverSeg and SENet. We use a batch size of 4 and the same set of data augmentation transforms as the ones used for *Tyche-TS* to encourage within task and across task diversity. Train-

Augmentations	$p$	Parameters
Random Affine	0.25	degrees $\in [-25, 25]$ translate $\in [0, 0.1]$ scale $\in [0.9, 1.1]$
Brightness Contrast	0.5	brightness $\in [-0.1, 0.1]$ , contrast $\in [0.5, 1.5]$
Elastic Transform	0.8	$\alpha \in [1, 2.5]$ $\sigma \in [7, 9]$
Sharpness	0.25	sharpness = 5
Flip Intensities	0.5	None
Gaussian Blur	0.25	$\sigma \in [0.1, 1.0]$ k=5
Gaussian Noise	0.25	$\mu \in [0, 0.05]$ $\sigma \in [0, 0.05]$

(a) In-Task Augmentation

Augmentations	$p$	Parameters
Random Affine	0.5	degrees $\in [0, 360]$ translate $\in [0, 0.2]$ scale $\in [0.8, 1.1]$
Brightness Contrast	0.5	brightness $\in [-0.1, 0.1]$ , contrast $\in [0.8, 1.2]$
Gaussian Blur	0.5	$\sigma \in [0.1, 1.1]$ k = 5
Gaussian Noise	0.5	$\mu \in [0, 0.05]$ $\sigma \in [0, 0.05]$
Elastic Transform	0.5	$\alpha \in [1, 2]$ $\sigma \in [6, 8]$
Sharpness	0.5	sharpness = 5
Horizontal Flip	0.5	None
Vertical Flip	0.5	None
Sobel Edges Label	0.5	None

(b) Task Augmentation

Table 6. **Set of augmentations used to train Tyche-TS.** We distinguish between augmentations aimed at increasing the diversity inside a task (Top) and the augmentations aimed at increasing the diversity of tasks (Bottom). An augmentation is applied with probability  $p$  (second column).

ing UniverSeg on the same datasets as *Tyche* improves performances compared to the official UniverSeg release, as shown in Figure 13.

**Specialized benchmarks.** For the specialized models (CIDM, PhiSeg, and Probabilistic UNet), we train a model for each task, for a total of 20 tasks. For each task, we train three model variants, one for each different data augmentation scheme, shown Table 8. We select the model with the data augmentation strategy that does best on the *out-of-distribution* validation set. We use a batch size of 4. For CIDM and Probabilistic UNet, we use the official PyTorch release. We found Probabilistic UNet particularly unstable to train on some datasets when applying augmentations. To

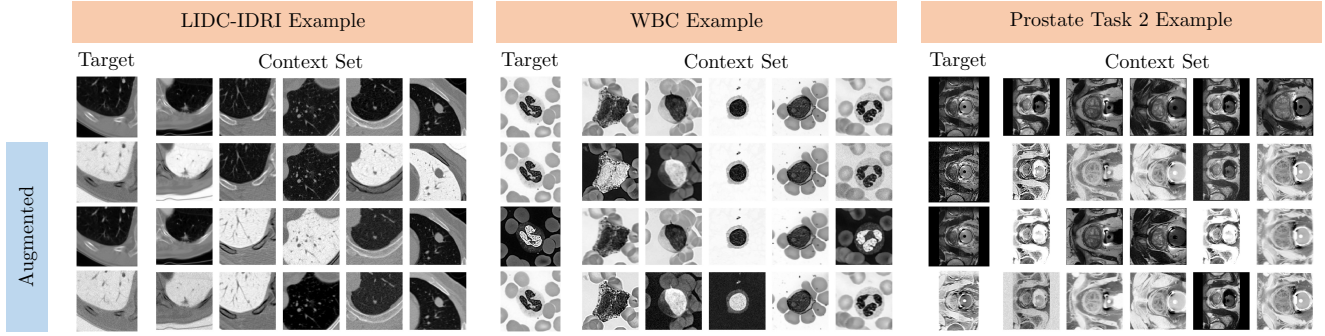


**Figure 12. Example Augmentations for Tyche-IS.** We show for samples from different datasets how three new segmentation candidates are generated. Starting from the top row, augmentations are applied to both the target and context set to obtain new prediction. Each row represents a new target-context pair. We do not show the corresponding labels as for *Tyche-IS*, we only augment with intensity-based transforms.

<b>Tyche-IS Augment.</b>	$p$	Parameters
Gaussian Blur	0.25	$\sigma \in [0.1, 1.0]$ $k = 5$
Gaussian Noise	0.25	$\mu \in [0, 0.05]$ $\sigma \in [0, 0.05]$
Flip Intensities	0.5	None
Sharpness	0.25	sharpness=5
Brightness Contrast	0.25	brightness $\in [-0.1, 0.1]$ , contrast $\in [0.5, 1.5]$

**Table 7. Augmentations used for Tyche-IS.** We focus on intensity transforms, to avoid inverting the prediction. For each image, an augmentation is sampled with probability  $p$ .

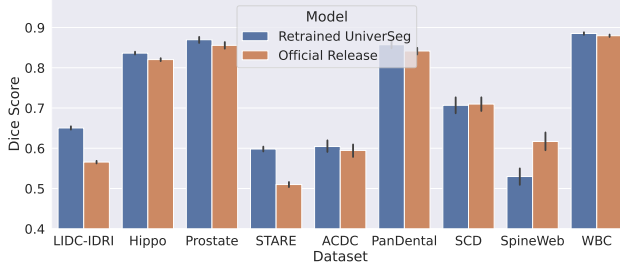


**Figure 13. Improvement of UniverSeg by training with more data.** By training UniverSeg on more data, we obtain a better average Dice score than the official UniverSeg release.

avoid diverging loss values, we had to initialize the Probabilistic UNet models from versions trained on datasets without augmentation. For PhiSeg, the official TensorFlow release was unstable, and we worked with the authors to run a more recent PyTorch version of their code. Per the authors’ request, we smooth the predicted segmentations of CIDM to remove irregularities in the final segmentations.

**Interactive Methods.** We use the SAM-Med2D and SAM as interactive segmentation baselines. In our setting, user

interaction is not available. We simulate it by averaging the ground truth labels from the context set and sample clicks and bounding boxes from averages.

We use SAM-Med2D’s official release as it is an adaptation of SAM exclusively meant for 2D medical image segmentation tasks. We found empirically that SAM-Med2D performs best when 3 positive and 2 negative clicks are sampled. For the negative clicks, we sample areas inside the bounding box that are not covered by the context set.

We also fine-tune SAM on our data. We sample 5 positive clicks and 5 negative clicks uniformly. We also provide a bounding box and the average of the context label maps as input.

## C. Advantages of candidates loss

### C.1. Intuition behind best candidate loss

The best candidate loss only evaluates the candidate that yields the lowest loss. We provide intuition for this loss function (Figure 14).

Given as input a target  $x^t$  and a context  $\mathcal{S}^t$ , the model outputs  $K$  segmentation candidates  $\hat{y}_j$ . Despite potentially high target ambiguity, for each training iteration we use only one annotation  $y_r^t$ .

The loss element  $l(\hat{y}_k, y_r^t)$  captures volume overlap between a candidate prediction  $\hat{y}_k$  and the rater annotation  $y_r^t$ . If a regular loss is used across all predictions, then *each* prediction tends towards the lowest expect cost over the space of possible segmentations for that image, leading to a mean segmentation among raters. This is particularly harmful when target ambiguity is high (high rater disagreement). Then, the mean segmentation may be very different than any one rater and may not be representative of the ambiguity. For the best candidate loss, the model is encouraged to make very different guesses for different segmentation candidates. This increases the chance that one prediction

Augmentation Set 1		
	$p$	Parameters
None	1	None
(a) No Augmentation. The images are given to the specialized model as is.		
Light Augmentation		
Gaussian Blur	0.5	$\sigma \in [0.1, 1.5]$ $k = 7$
Gaussian Noise	0.5	$\mu \in [0, 0.1]$ $\sigma \in [0, 0.1]$
Variable Elastic Transform	0.25	$\alpha \in [1, 2]$ $\sigma \in [6, 8]$
(b) Light Augmentation. Gaussian blur, Gaussian noise, elastic transforms are each applied to the target with probability $p$ .		
Heavy Augmentation		
Gaussian Blur	0.5	$\sigma \in [0.1, 1.5]$ $k = 7$
Gaussian Noise	0.25	$\mu \in [0, 0.1]$ $\sigma \in [0, 0.1]$
Elastic Transform	0.25	$\alpha \in [1, 2]$ $\sigma \in [6, 8]$
Random Affine	0.5	degrees $\in [0, 360]$ translate $\in [0, 0.2]$ scale $\in [0.8, 1.1]$
Brightness Contrast	0.5	brightness $\in [-0.1, 0.1]$ , contrast $\in [0.5, 1.5]$
Horizontal Flip	0.5	None
Vertical Flip	0.5	None
Sharpness	0.5	sharpness = 5
(c) Full Set of Augmentations. To form the last augmentation set, we add the following transforms: Affine transform, Sharpness, Brightness and Flips.		

Table 8. **Set of Augmentations used to train the specialized benchmarks.** For evaluation, we select the model with the training augmentations that does best on the *out-of-distribution* validation set.

matches the rater being used as ground truth at that iteration.

## C.2. Distribution loss function

Since *Tyche-TS* enables multiple candidates that can coordinate with one another, we can employ loss functions that apply to a collection of raters and predictions. We demonstrate this concept by fine-tuning *Tyche-TS*, using a  $GED^2$  loss function.

Figure 15 shows that the corresponding model produces samples with lower  $GED^2$ , as expected.

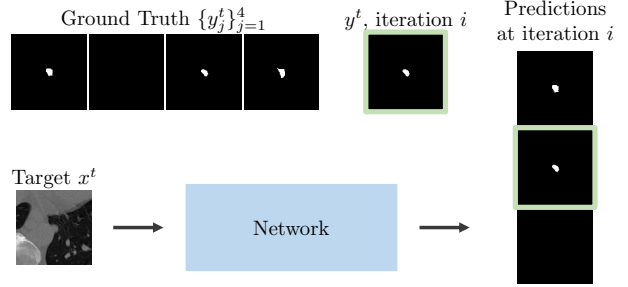


Figure 14. **Best candidate Loss Explanation.** Because of ambiguity in the target, there are multiple plausible ground truths. With a standard Dice loss, all the candidates segmentation converge to the mean segmentation. The best candidate loss enables the model to explore different plausible segmentation, since even one proposal matching the rater segmentation used at that iteration leads to a good loss value.

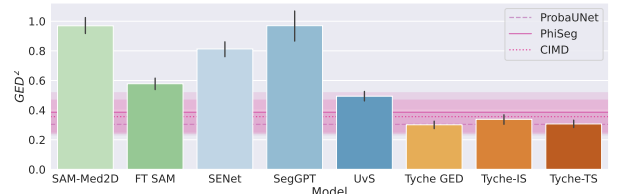


Figure 15. **Tyche-TS with GED loss** (yellow) improved test-time GED performance (lower is better).

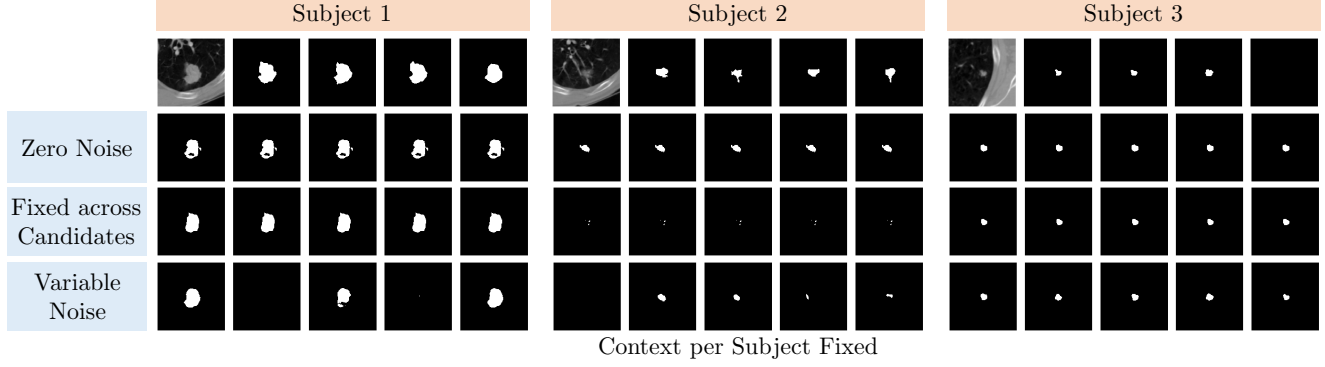
## D. Tyche Analysis

We first analyse the different components that lead to variability in *Tyche-TS*: the noise, the context set, the number of prediction in on forward pass, and the *SetBlock* mechanism. We then investigate how the size of the context set and the number of predictions impact performances. For *Tyche-IS*, we investigate different plausible sets of augmentations to apply. Finally, we show that *Tyche* can produce good results even in data scarcity settings when a stochastic methods trained solely on a few samples would have limited performance.

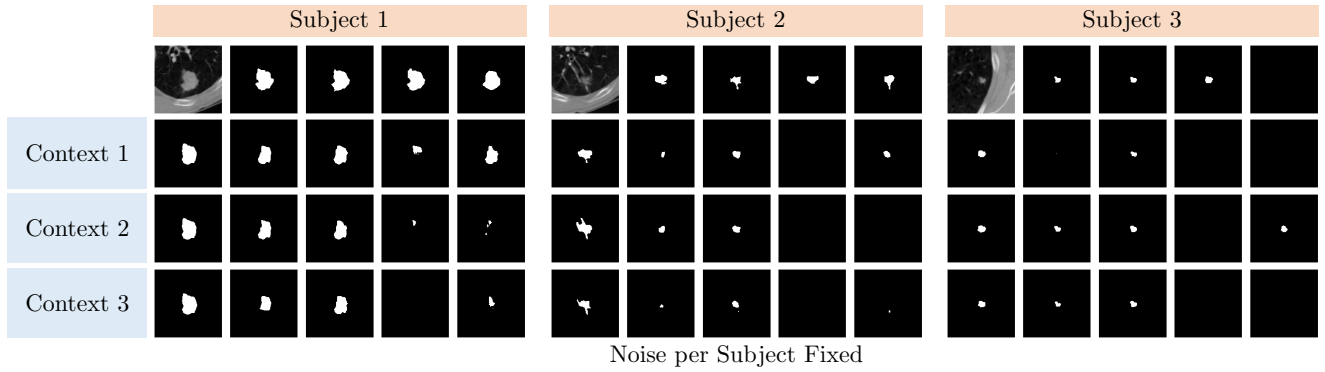
### D.1. Diversity from noise

Figure 16 shows how three predictions vary depending on three noise variants: zero-noise, constant noise across candidates, and variable noise. Both zero noise and constant noise lead systematically to identical segmentation candidates. For each example of segmentation candidates, the context set is fixed.

Figure 18 shows that setting the noise to 0 for *Tyche-TS* produces similar performances to UniverSeg, both for GED and best candidate Dice score.



**Figure 16. Prediction variability as a function of injected noise.** Examples of predictions for three subjects with three different types of input noise. Top to Bottom: zero noise, Gaussian noise constant across segmentation candidates, and randomly sampled Gaussian noise. The context set is fixed. With random noise as an input *Tyche* can output diverse segmentation candidates.



**Figure 17. Prediction variability as a function of the context set.** The context set significantly contributes to the variability of the output. For three different subjects, we show how the corresponding segmentation candidates are affected by different context sets. The random Gaussian noise given as input is fixed for each set of candidates.

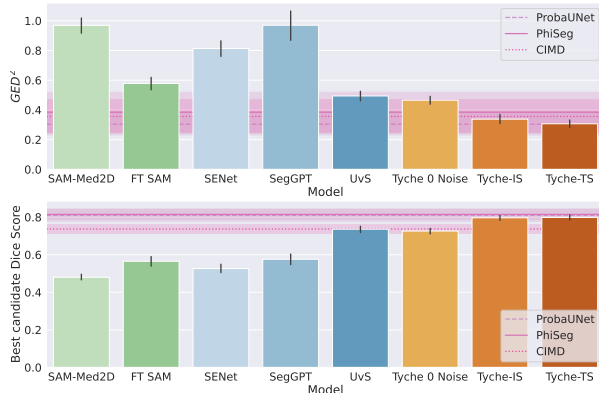


**Figure 18. *Tyche-TS* with no noise gives similar results to UniverSeg.** Setting the noise to 0 for *Tyche-TS* gives similar best candidate Dice score and similar  $GED^2$  to UniverSeg. Top: Generalized Energy Distance. Bottom: Best candidate Dice Score.

## D.2. Diversity from context

Figure 17 shows example predictions for three subjects and three context sets. Different contexts lead to different predictions, even if the noise is the same, sometimes drastically. For instance, the predictions for subject 1 and context 3 contain a candidate with no annotations.

## D.3. Diversity in the number of predictions

While *Tyche-IS* predicts each segmentation sample sequentially, *Tyche-TS* has a one-shot mechanism that predicts all the candidates at once. One may wonder how the number of predictions requested at inference impacts the output of *Tyche-TS*. Figure 19 shows that with the number of prediction set to 1, *Tyche-TS* loses a lot of its diversity compared to 5 predictions.

This is also shown quantitatively in Figure 21, where Generalized Energy Distance decreases as the number of predictions increases.

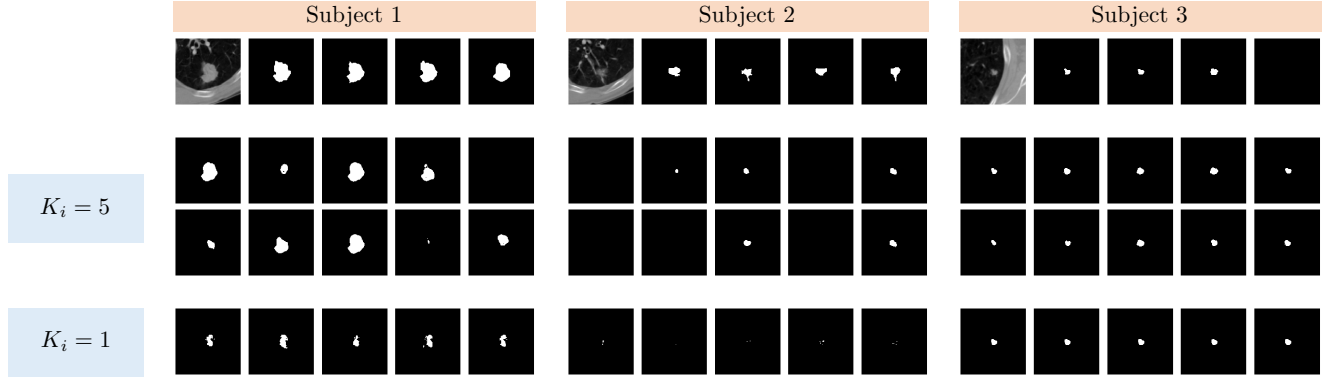


Figure 19. **Setting a number of predictions larger than 1 allows for more diversity.** The outputs of *Tyche-TS* are a lot more uniform when the number of prediction is set to 1 than when it is set to 5.

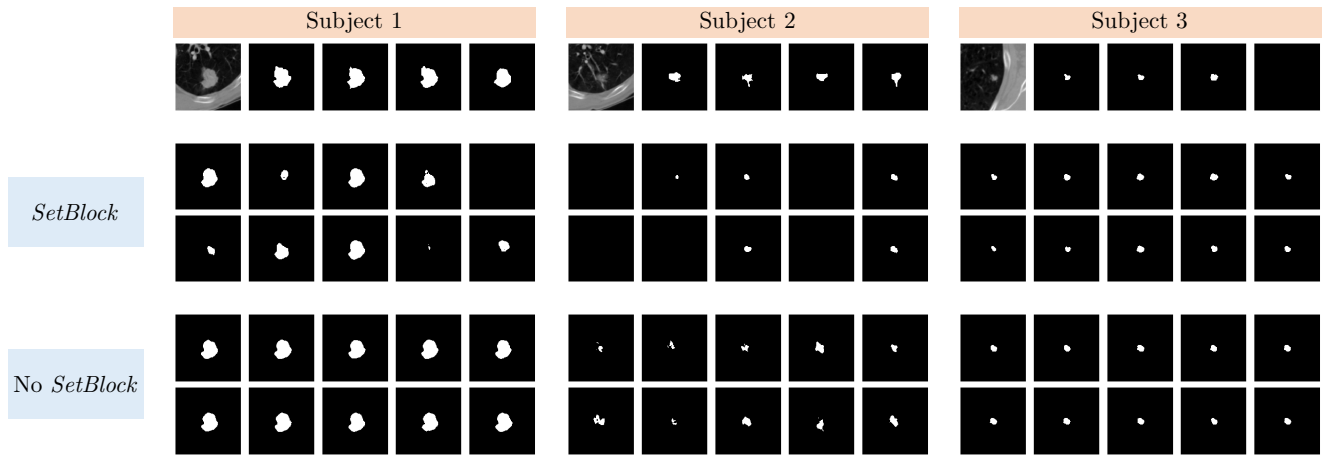


Figure 20. **Removing the SetBlock leads to less diversity in the output.** The segmentation candidates output by *Tyche-TS* are more diverse than the candidates of a *Tyche* model trained without the *SetBlock* interaction.

#### D.4. Diversity from the SetBlock

*Tyche-TS* has an intrinsic mechanism to encourage the segmentation candidates to be diverse: *SetBlock*. Figure 20 visually compares the segmentations predicted with the mechanisms and the segmentations predicted by a *Tyche* model trained without the *SetBlock*. Without the *SetBlock*, the predictions output by *Tyche* are a lot less diverse.

#### D.5. Size of the Context Set

Generally, a larger context set improves performances. Figure 22 shows that Generalized Energy Distance improves as the size of the context set increases. However, the improvement decreases beyond 16 samples.

#### D.6. Augmentations

We study different augmentation for *Tyche-IS* and how they influence the quality of predictions. We consider four settings: no augmentation, only light augmentation such as

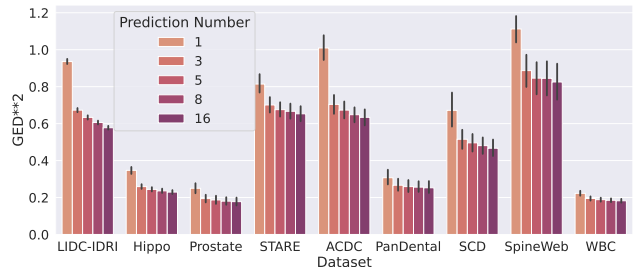


Figure 21. **GED<sup>2</sup> for Tyche as a function of the number of predictions,  $K_i$ .** Performances improve with the number of prediction but with diminishing returns.

Gaussian Noise and Gaussian Blur, described Table 7, the *Tyche-IS* augmentations shown Table 7 and the *Tyche-IS* with slightly stronger parameters, shown Table 9. The results are shown in Figure 23 both aggregated across datasets and for each dataset individually. Overall, adding augmen-

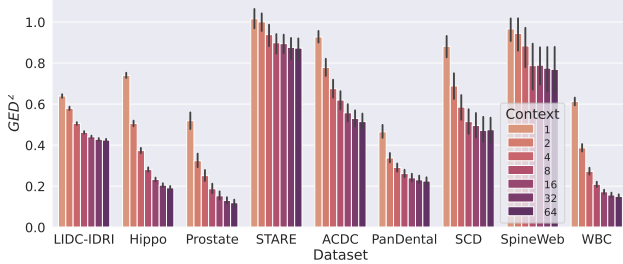


Figure 22.  $GED^2$  for Tyche as a function of the inference context size. Performances improve as the context size increases but with diminishing returns.

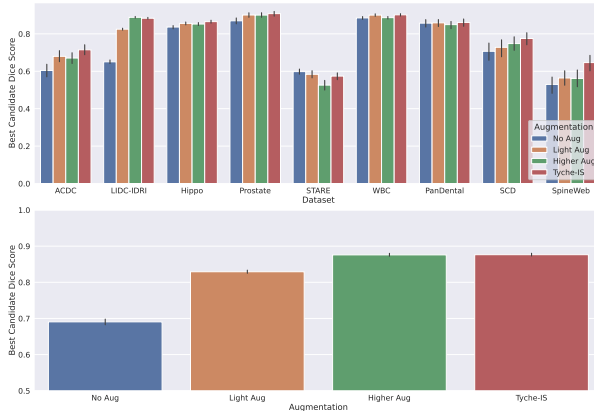


Figure 23. Performance of different augmentation schemes for Tyche-IS. We consider four augmentations: none, light, the one used in Tyche-IS and a stronger version of the later. Top: Per Dataset. Bottom: Overall. The one that we selected for Tyche-IS is the most promising.

Tyche-IS High Aug.	$p$	Parameters
Gaussian Blur	0.25	$\sigma \in [0.5, 1.0]$ $k = 5$
Gaussian Noise	0.5	$\mu \in [0.4, 0.5]$ $\sigma \in [0.1, 0.2]$
Flip Intensities	0.5	None
Sharpness	0.25	sharpness=5
Brightness Contrast	0.25	brightness $\in [-0.1, 0.1]$ , contrast $\in [0.5, 1.5]$

Table 9. High augmentations used to validate Tyche-IS. We focus on intensity transforms, to avoid inverting the prediction. For each image, an augmentation is sampled with probability  $p$ .

tations improves the best candidate Dice score. However, it can degrades the quality of the predictions, for instance for STARE. The augmentation we selected for Tyche-IS is the most promising so far, without requiring inversion of the transform applied.

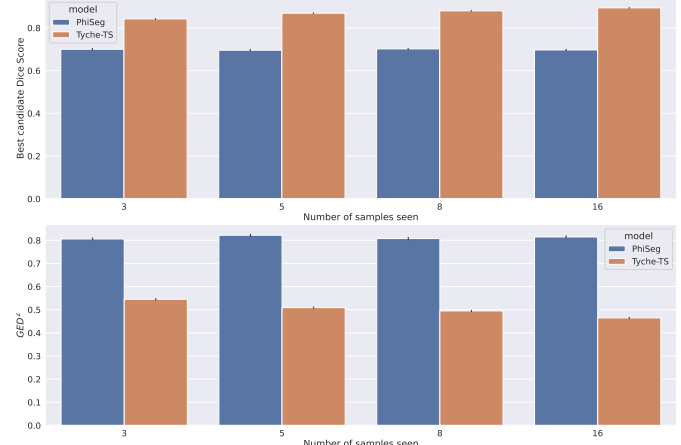
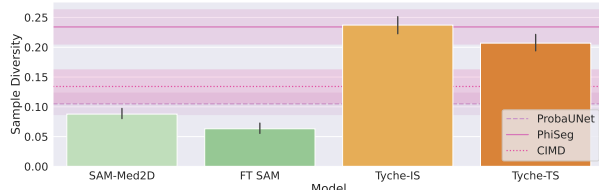


Figure 24. Few-Shot Regime. Comparison between Tyche-TS and PhiSeg trained on the few-shot examples. PhiSeg fails to learn from very few samples both on max. Dice score and GED, compared to Tyche.

## D.7. Few Shot Regime

We train PhiSeg on a subset of LIDC-IDRI,  $\tilde{\mathcal{S}}$ , and examine how this network generalizes compared to Tyche, where the context set is  $\tilde{\mathcal{S}}$ . We investigate four few-shot settings: 3, 5, 8 and 16. For each, we train 30 PhiSegs: 10 seeds to account for variability in our samples and three data augmentation regimes (none, light, normal). For each seed and each few-shot setting, we select the PhiSeg that does best on the validation set. Figure 24 shows that Tyche can leverage the data available much more effectively than PhiSeg, which fails to learn with so little samples.



**Figure 25. Sample Diversity on Multi-Annotator Data.** Since the sample diversity of the deterministic methods is 0, we do not show them here. *Tyche-IS* produces the most diverse samples, while Fine-Tuned SAM has very low diversity, despite varying clicks and bounding box locations. Higher is better.

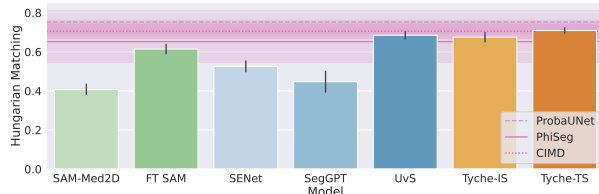


**Figure 26. Hungarian Matching on Multi-Annotator Data.** Both *Tyche-IS* and UniverSeg perform well. *Tyche-TS* performs best. Higher is better.

## E. Further Evaluation

### E.1. Performances on other Metrics

Evaluating the quality of different predictions can be challenging especially when different annotators are available. We proposed best candidate Dice score and Generalized Energy Distance. Some also analysed sample diversity [95], and Hungarian Matching [68, 133]. Sample diversity consists in measuring the agreement between candidate predictions  $\hat{\mathcal{Y}}$ , rewarding most diverse sets of candidates:

$$D_{SD}(\hat{\mathcal{Y}}) = \mathbb{E}[d(\hat{p}, \hat{p}')], \quad (17)$$

where  $\hat{p}, \hat{p}' \sim \hat{\mathcal{Y}}$  and  $d(\cdot, \cdot)$  is Dice score. One limitation of this metric is that it blindly rewards diversity without taking into account the natural ambiguity in the target. Ideally, when there is high ambiguity in the target, the samples are very diverse, and inversely, when there is low ambiguity, the segmentation candidates are not diverse.

In the context of stochastic predictions, Hungarian Matching [70] consists in matching the set of predictions with the set of annotations, so that an overall metric is minimized. We use negative Dice score. One limitation of this method is that it has to be adapted when the number of annotators does not match the number of prediction. The most widely used fix is to artificially inflate the number of predictions and the number of annotations to reach the least common multiple [68]. We use this strategy here as well.

Figures 25 and 26 show the performances for sample diversity and Hungarian Matching respectively.

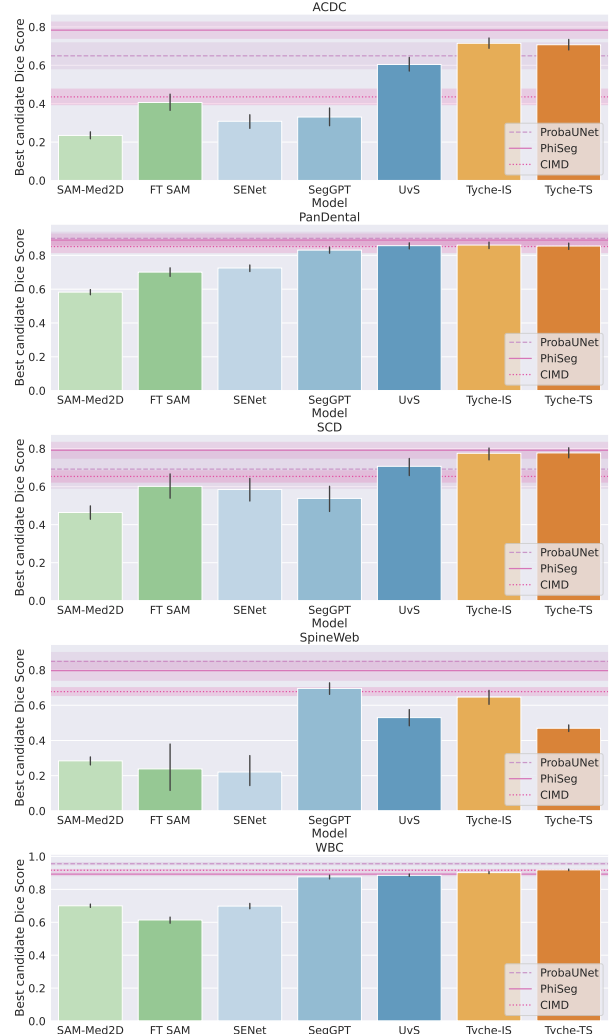


**Figure 27. Best candidate Dice score for the Single-Annotator Datasets.** Top to Bottom: ACDC, PanDental, SCD, SpineWeb and WBC. *Tyche* performs well in general except for SpineWeb.

### E.2. Per Dataset Results

We show for each dataset and each method the best candidate Dice score. We also show for *Tyche* and the different benchmarks Generalized Energy Distance, Hungarian Matching and Sample Diversity for the datasets with multiple annotations.

**Best candidate Dice Score.** Figure 27 shows the best candidate Dice score for the single-annotator datasets. *Tyche* performs well across datasets. Both versions of *Tyche* seem to dominate both types of benchmarks and be comparable to the upper bounds, except for one dataset: SpineWeb. We hypothesize that part of the performance drop is due to the nature of the structure to segment in SpineWeb: individual vertebra. Most of our training data contains single struc-

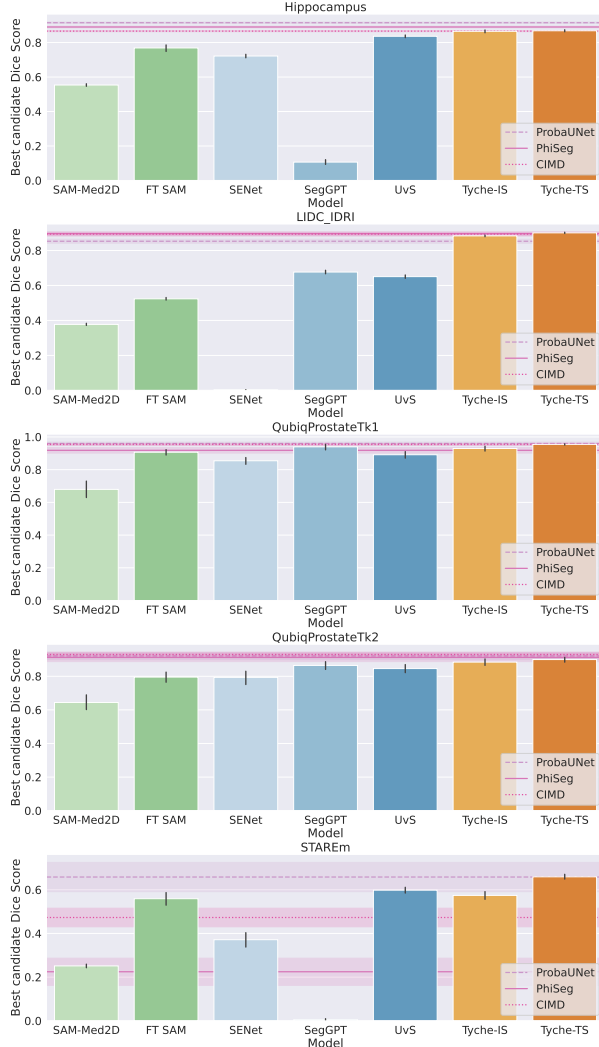


Figure 28. **Best candidate Dice Score for Multi-Annotator Datasets** Top to bottom: Hippocampus, LIDC-IDRI, Prostate Task 1, Prostate Task 2 and STARE. *Tyche* performs well across datasets. (Higher is better.)

tures to segment.

Figure 28 shows the best candidate Dice score for the multi-annotator datasets. Similar conclusions can be drawn as for the single-annotator data. Some benchmarks are particularly sensitive to the data they are evaluated on, for instance SegGPT. This method performs really well on the Prostate data but quite poorly on the STARE and the Hippocampus data. We assume that because SegGPT was designed for images of 448x448, our images of dimension 128x128 might affect performances.

**Generalized Energy Distance.** Figure 29 shows Generalized Energy distance for the multi-rater datasets.

**Hungarian Matching.** Figure 30 shows the Hungarian

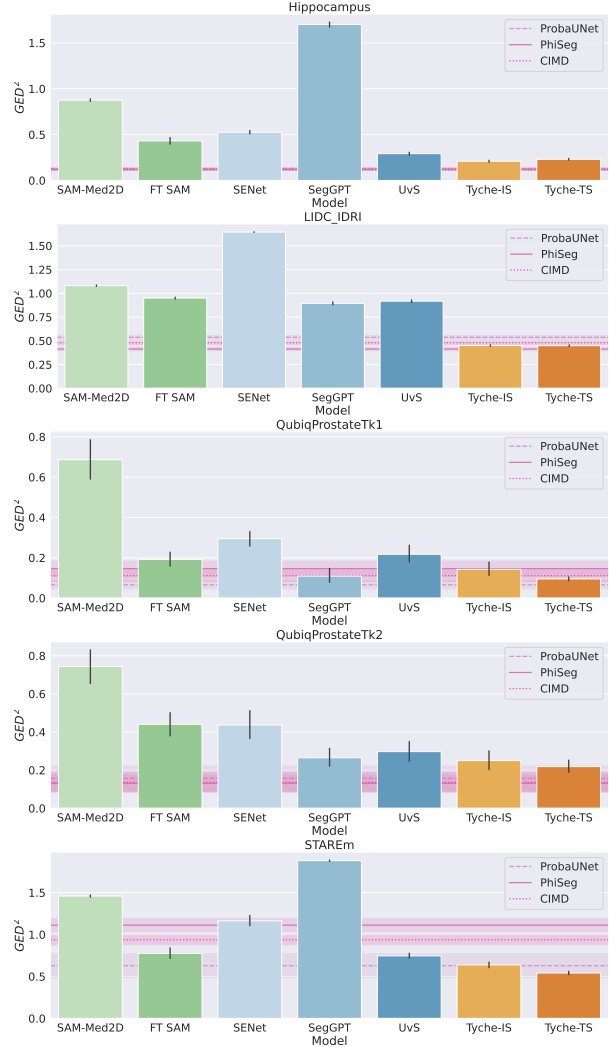


Figure 29. **Generalized Energy Distance for Multi-Annotator Datasets.** Top to bottom: Hippocampus, LIDC-IDRI, Prostate Task 1, Prostate Task 2 and STARE. *Tyche* performs well across datasets. (Lower is better.)

Matching metric for the multi-rater datasets. We find that UniverSeg performs particularly well. We suspect that because we have to artificially duplicate our samples to compute this metric, the resulting scenario favors methods that are closer to the mean.

**Sample Diversity.** Figure 31 shows sample diversity for the multi-annotator datasets. We only show the sample diversity for the methods outputting more than one segmentation candidate. For UniverSeg, SegGPT and SENet, the sample diversity is trivially 0.

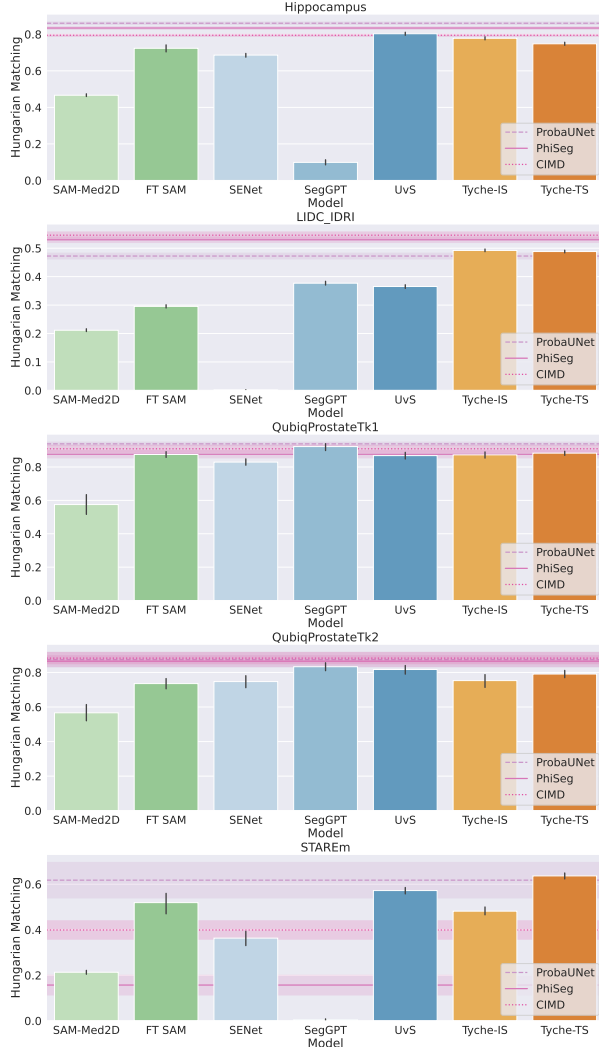


Figure 30. **Hungarian Matching Dice for Multi-Annotator Datasets.** Top to bottom: Hippocampus, LIDC-IDRI, Prostate Task 1, Prostate Task 2 and STARE. *Tyche* performs well across datasets. (Higher is better.)

### E.3. Additional Visualizations

We show additional visualization for *Tyche* frameworks as well as all the benchmarks.

**Single-Annotator Data** Visualizations for ACDC are shown Figure 32. We show two PanDental examples Figure 34 and Figure 35, one for each task. We show an example for SpineWeb Figure 33 and one for WBC Figure 37.

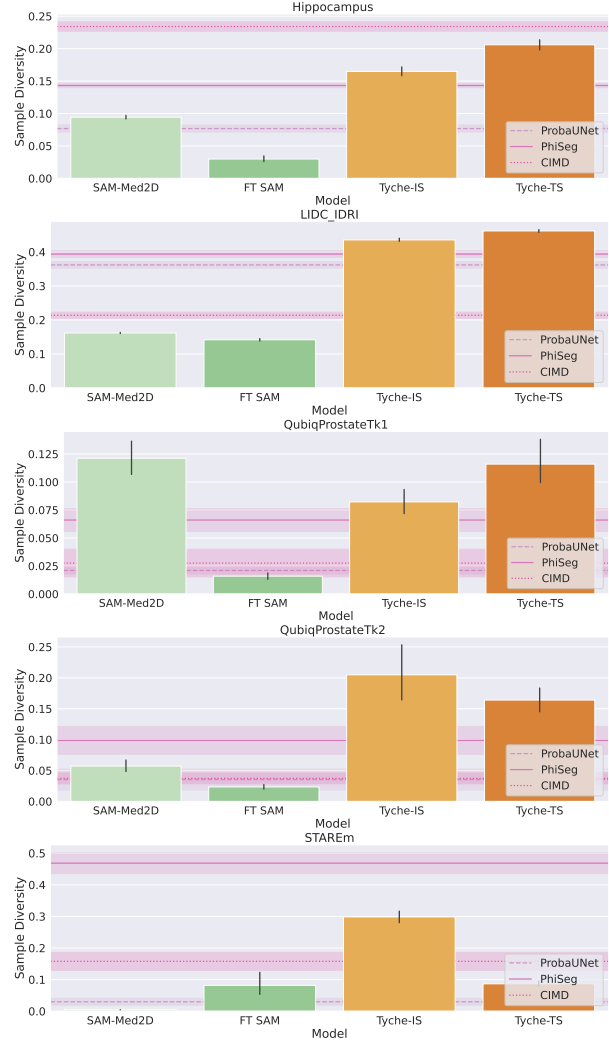


Figure 31. **Sample Diversity for Multi-Annotator Datasets.** Top to bottom: Hippocampus, LIDC-IDRI, Prostate Task 1, Prostate Task 2 and STARE. *Tyche* performs well across datasets. We only show methods with diversity greater than 0. (Higher is better.)

**Multi-Annotator Data** We show an example prediction for the Hippocampus data Figure 38 and one example prediction for STARE in Figure 39. We provide visualizations for each Prostate task Figures 40 and 41 respectively. Finally, we give two example visualizations for LIDC-IDRI Figures 42 and 43.

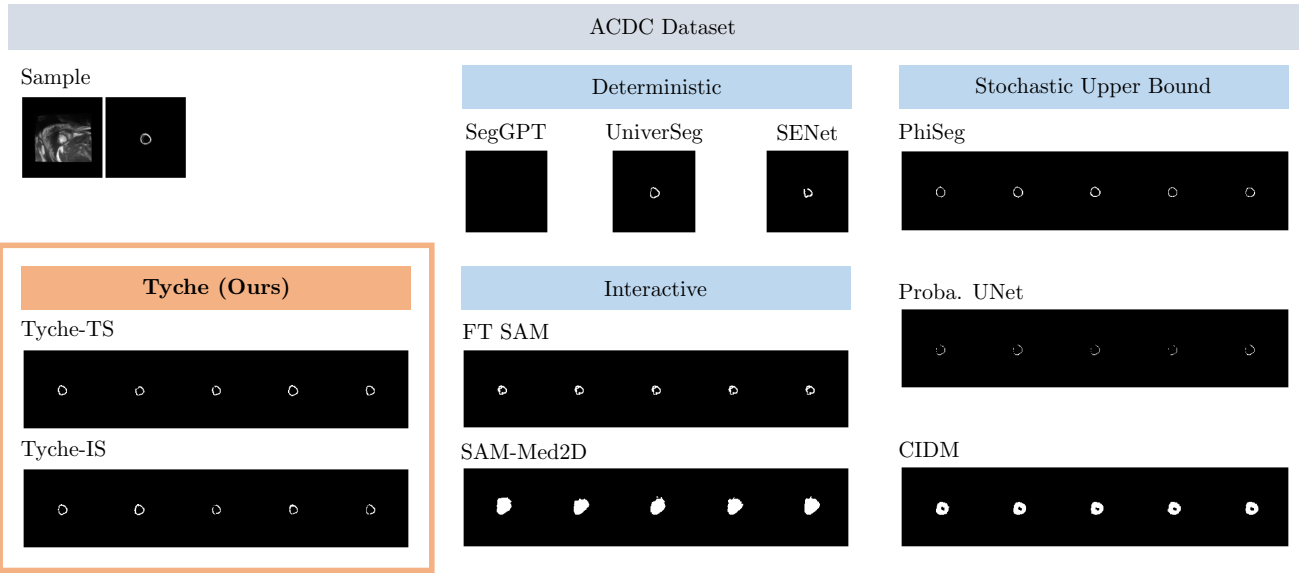


Figure 32. Example Prediction for ACDC.

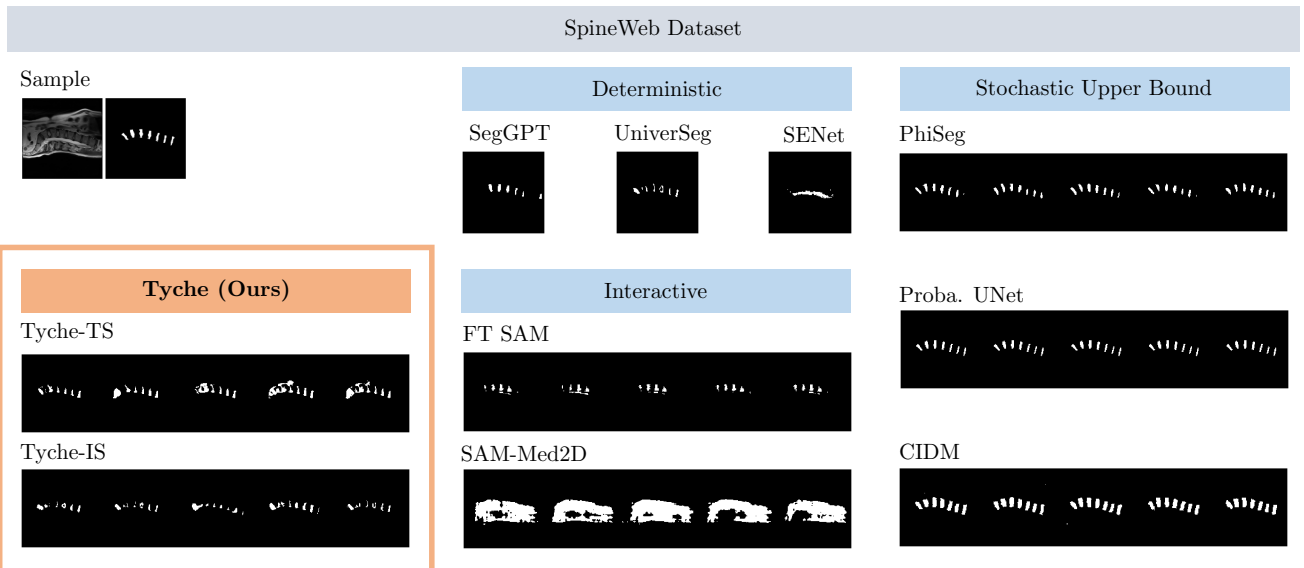


Figure 33. Example Prediction for SpineWeb.

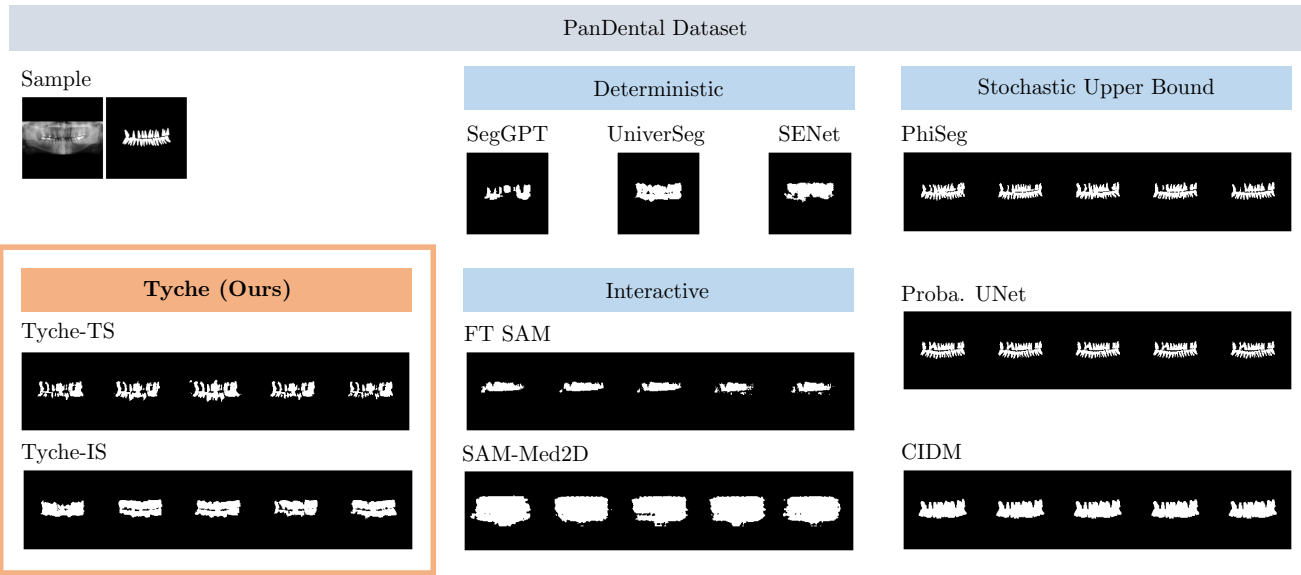


Figure 34. Example Prediction for PanDental, task 1.

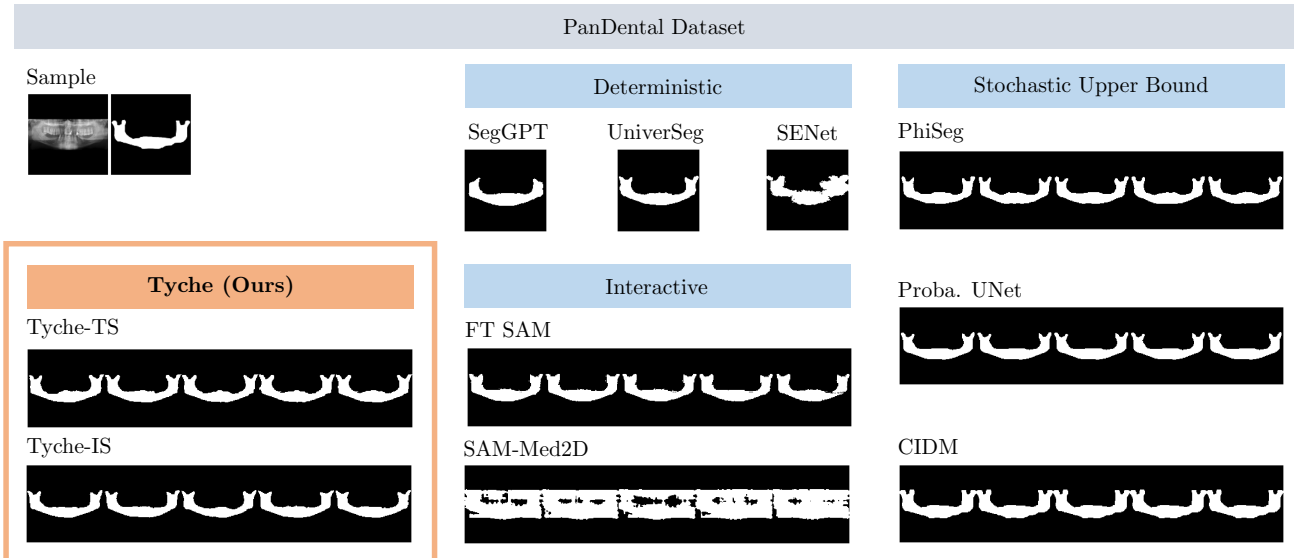


Figure 35. Example Prediction for PanDental, task 2.

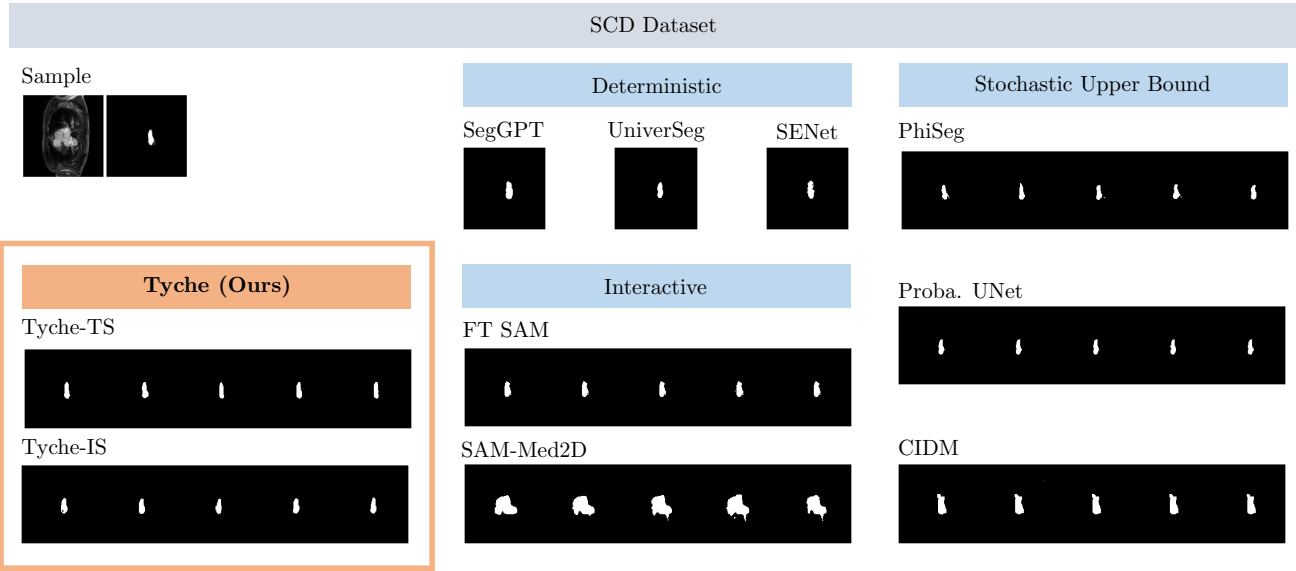


Figure 36. Example Prediction for SCD.

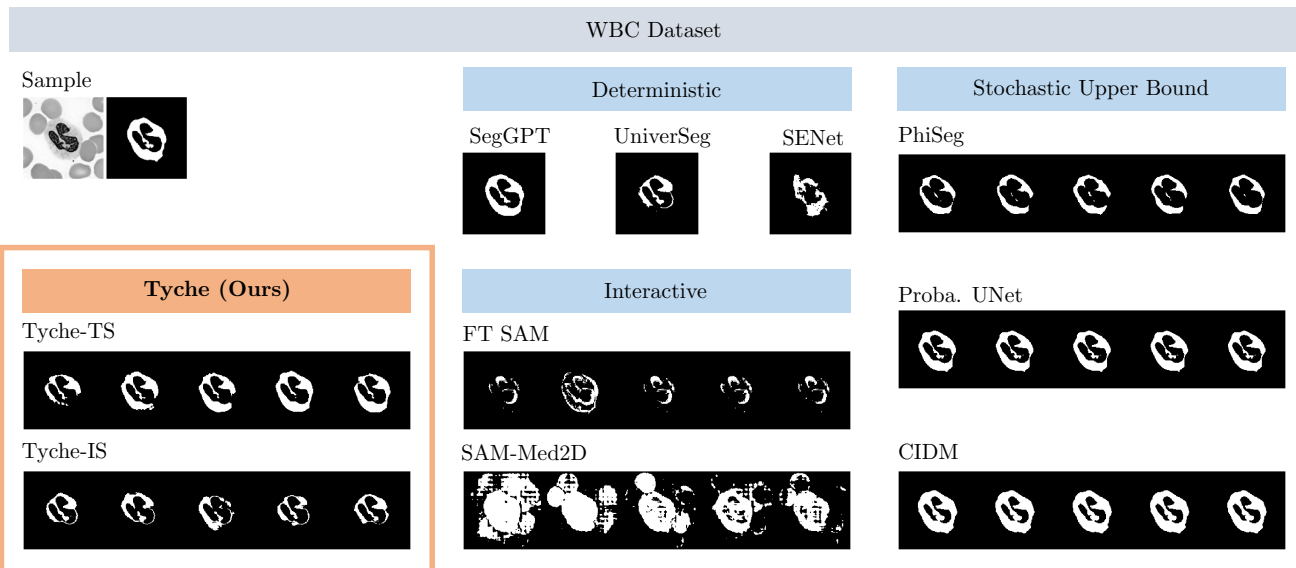


Figure 37. Example Prediction for WBC.

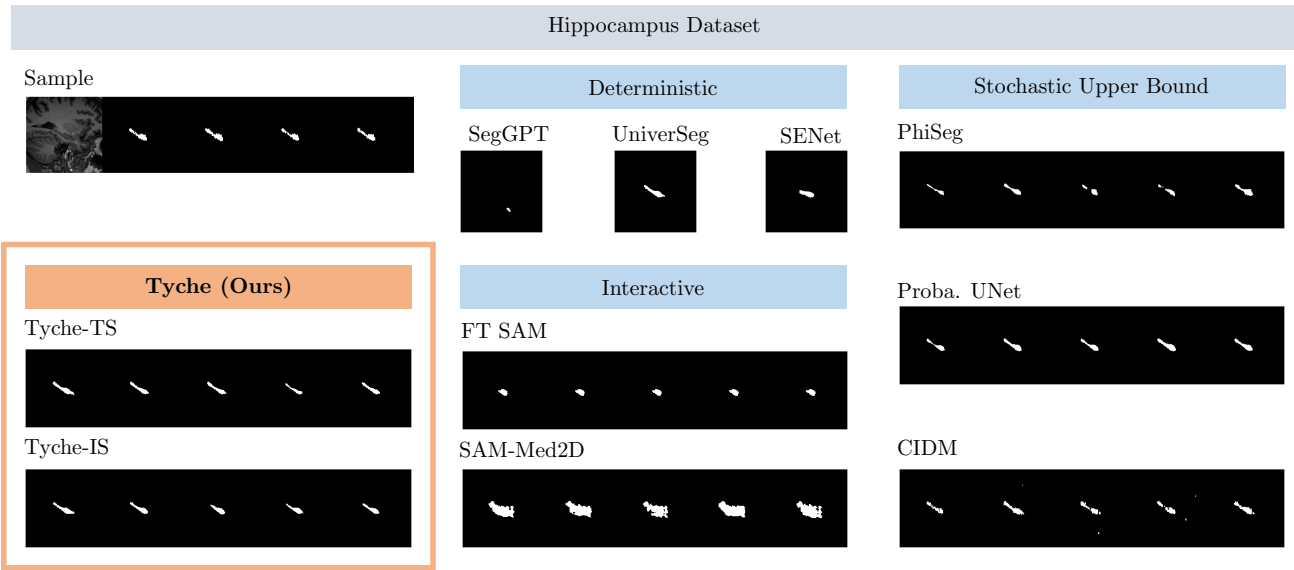


Figure 38. Example Prediction for Hippocampus.

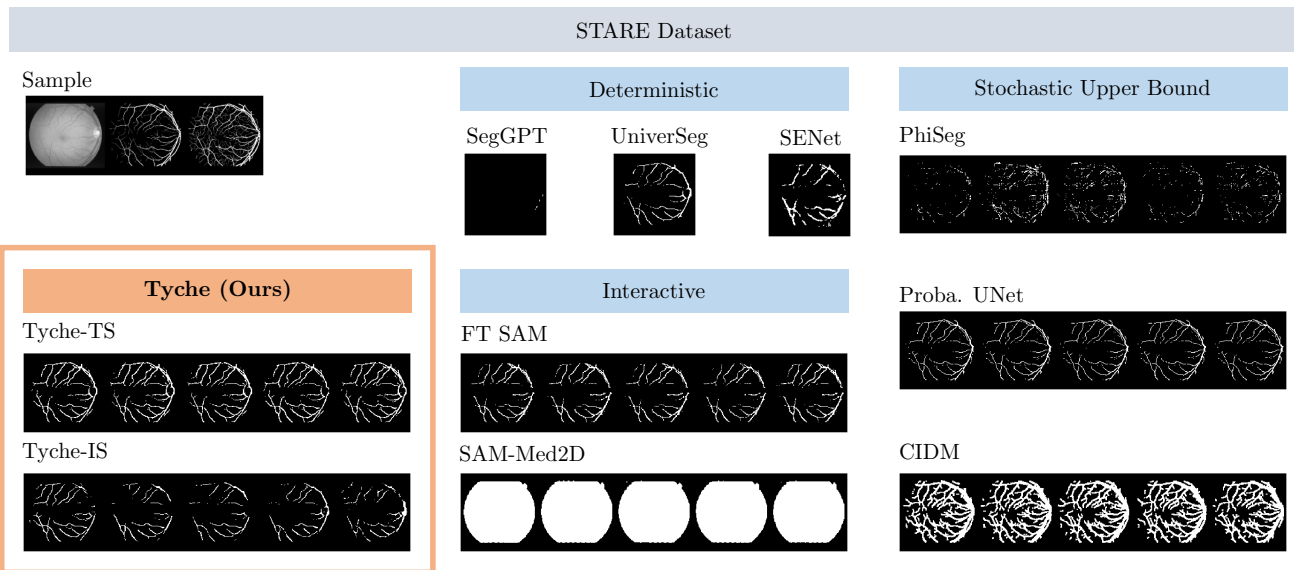


Figure 39. Example Prediction for STARE.

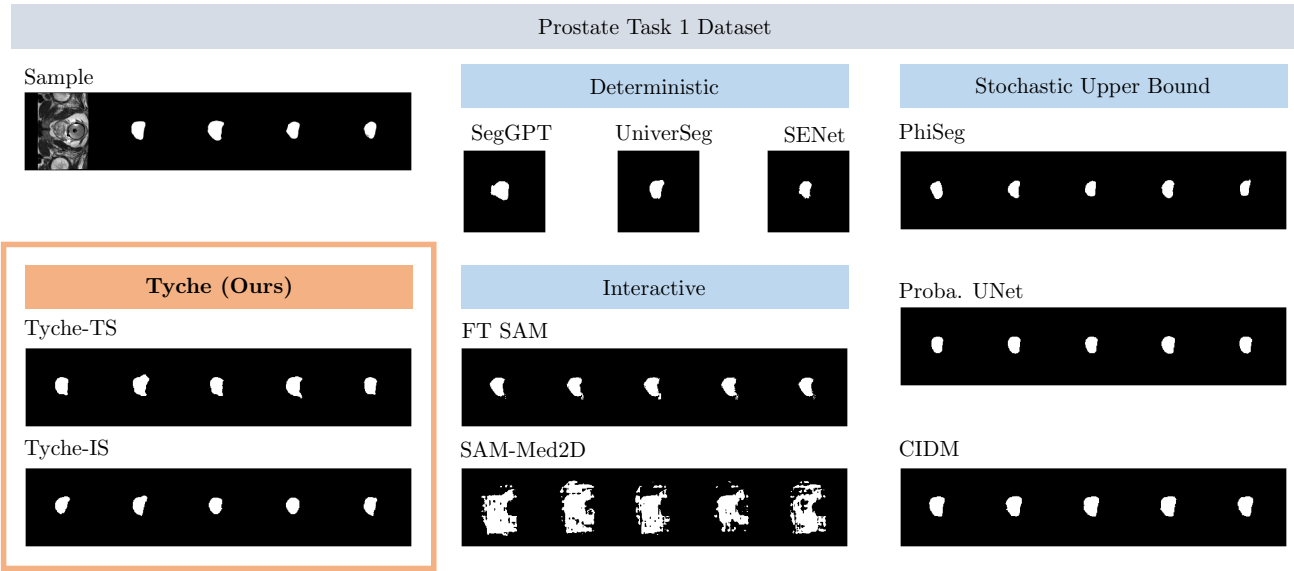


Figure 40. Example Prediction for Prostate Task 1.

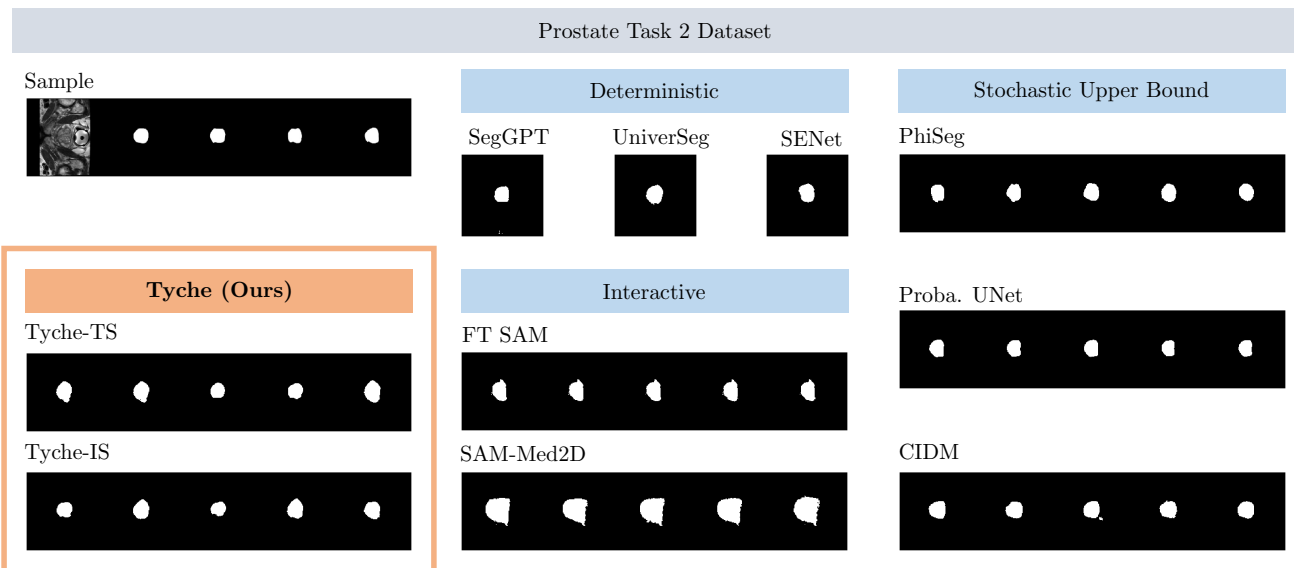


Figure 41. Example Prediction for Prostate Task 2.

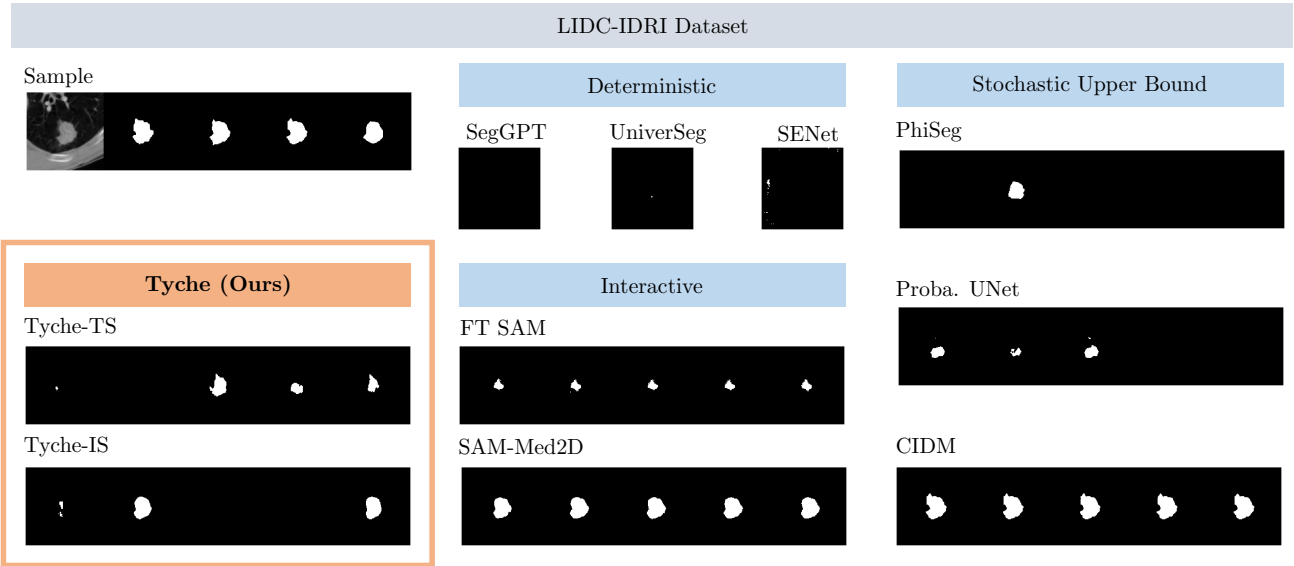


Figure 42. Example Prediction for LIDC-IDRI.

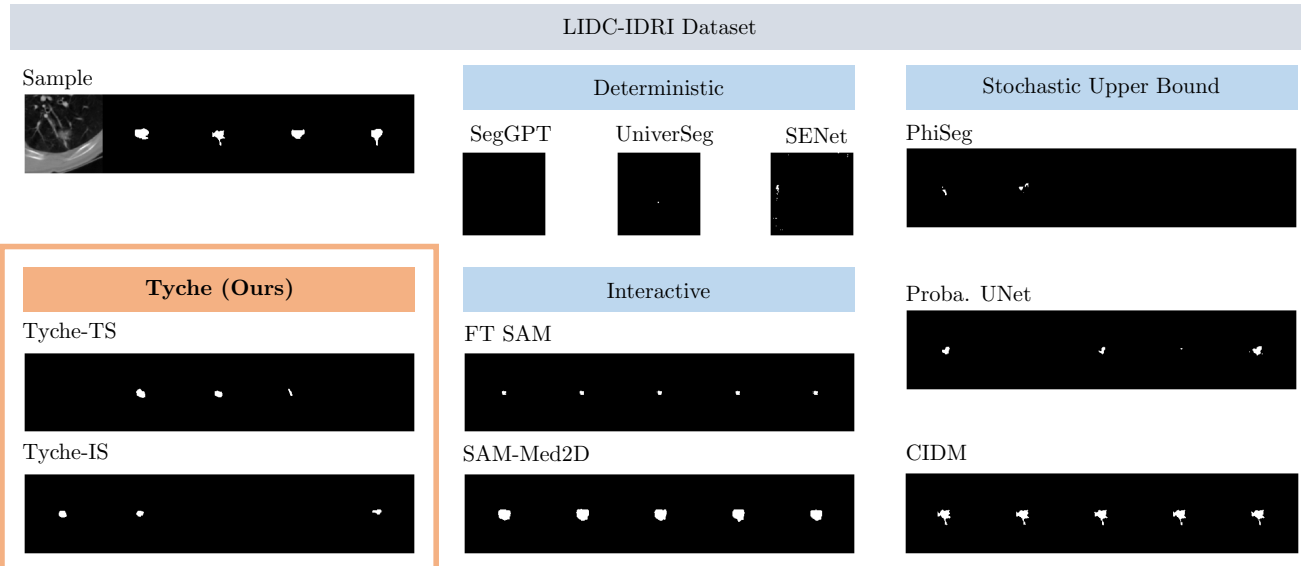


Figure 43. Example Prediction for LIDC-IDRI.

Dataset Name	Description	# of Scans	Image Modalities
ACDC [14]	Left and right ventricular endocardium	99	cine-MRI
AMOS [54]	Abdominal organ segmentation	240	CT, MRI
BBBC003 [83]	Mouse embryos	15	Microscopy
BBBC038 [20]	Nuclei images	670	Microscopy
BUID [2]	Breast tumors	647	Ultrasound
BrainDev. [37, 38, 72, 114]	Adult and Neonatal Brain Atlases	53	multi-modal MRI
BRATS [7, 8, 93]	Brain tumors	6,096	multi-modal MRI
BTCV [75]	Abdominal Organs	30	CT
BUS [136]	Breast tumor	163	Ultrasound
CAMUS [77]	Four-chamber and Apical two-chamber heart	500	Ultrasound
CDemris [56]	Human Left Atrial Wall	60	CMR
CHAOS [58, 60]	Abdominal organs (liver, kidneys, spleen)	40	CT, T2-weighted MRI
CheXplanation [110]	Chest X-Ray observations	170	X-Ray
CT-ORG[106]	Abdominal organ segmentation (overlap with LiTS)	140	CT
DRIVE [122]	Blood vessels in retinal images	20	Optical camera
EOPHTHA [27]	Eye Microaneurysms and Diabetic Retinopathy	102	Optical camera
FeTA [102]	Fetal brain structures	80	Fetal MRI
FetoPlac [10]	Placenta vessel	6	Fetoscopic optical camera
HMC-QU [28, 65]	4-chamber (A4C) and apical 2-chamber (A2C) left wall	292	Ultrasound
HipXRay [40]	Ilium and femur	140	X-Ray
I2CVB [78]	Prostate (peripheral zone, central gland)	19	T2-weighted MRI
IDRID [103]	Diabetic Retinopathy	54	Optical camera
ISLES [43]	Ischemic stroke lesion	180	multi-modal MRI
KiTS [42]	Kidney and kidney tumor	210	CT
LGGFlair [18, 91]	TCIA lower-grade glioma brain tumor	110	MRI
LiTS [16]	Liver Tumor	131	CT
LUNA [115]	Lungs	888	CT
MCIC [36]	Multi-site Brain regions of Schizophrenic patients	390	T1-weighted MRI
MSD [118]	Collection of 10 Medical Segmentation Datasets	3,225	CT, multi-modal MRI
NCI-ISBI [17]	Prostate	30	T2-weighted MRI
OASIS [46, 88]	Brain anatomy	414	T1-weighted MRI
OCTA500 [79]	Retinal vascular	500	OCT/OCTA
PanDental [1]	Mandible and Teeth	215	X-Ray
PAXRay [112]	Thoracic organs	880	X-Ray
PROMISE12 [82]	Prostate	37	T2-weighted MRI
PPMI [89]	Brain regions of Parkinson patients	1,130	T1-weighted MRI
ROSE [86]	Retinal vessel	117	OCT/OCTA
SCD [104]	Sunnybrook Cardiac Multi-Dataset Collection	100	cine-MRI
SegTHOR [74]	Thoracic organs (heart, trachea, esophagus)	40	CT
SpineWeb [138]	Vertebrae	15	T2-weighted MRI
ToothSeg [50]	Individual teeth	598	X-Ray
WBC [139]	White blood cell and nucleus	400	Microscopy
WMH [71]	White matter hyper-intensities	60	multi-modal MRI
WORD [85]	Organ segmentation	120	CT

Table 10. **Collection of datasets in MegaMedical 2.0.** The entry number of scans is the number of unique (subject, modality) pairs for each dataset.

Dataset Name	Description	# of Scans	Image Modalities
LIDC-IDRI [4]	Lung Nodules	1018	CT
QUBIQ [92]	Brain, kidney, pancreas and prostate	209	MRI T1, Multimodal MRI, CT
STARE [47]	Blood vessels in retinal images	20	Optical camera

Table 11. **Multi-Annotator Data.** The entry number of scans is the number of unique (subject, modality) pairs for each dataset.